SANDIA REPORT

SAND97–2092 • UC–404
Unlimited Release
Printed September 1997

Novel Low-Permittivity Dielectrics for Si-Based Microelectronics

J. P. Sullivan

Prepared by
Sandia National Laboratories
Albuquerque, New Mexico 87185 and Livermore, California 94550

Sandia is a multiprogram laboratory operated by Sandia Corporation, a Lockheed Martin Company, for the United States Department of Energy under Contract DE-AC04-94AL85000.

SF2900Q(8-81)

Issued by Sandia National Laboratories, operated for the United States Department of Energy by Sandia Corporation.

Available to DOE and DOE contractors from
Office of Scientific and Technical Information
P.O. Box 62
Oak Ridge, TN 37831

Prices available from (615) 576-8401, FTS 626-8401

Available to the public from
National Technical Information Service
U.S. Department of Commerce
5285 Port Royal Rd
Springfield, VA 22161

NTIS price codes
Printed copy: A03
Microfiche copy: A01

SAND97-2092
Unlimited Release
Printed September 1997

Distribution
Category UC-404

Novel Low-Permittivity Dielectrics for Si-Based Microelectronics

J. P. Sullivan

Advanced Materials and Device Sciences Department, 1153
Sandia National Laboratories
P.O. Box 5800
Albuquerque, NM 87185-1421

Abstract

The purpose of this laboratory-directed research and development (LDRD) project was to develop and assess novel low-permittivity dielectric materials for applications as interlevel dielectrics (ILDs) in Si-based microelectronics. There were three classes of materials investigated: (1) novel covalently-bonded ceramics containing carbon, boron, and/or nitrogen, (2) fluorinated SiO_2 (SiOF), and (3) plasma polymerized fluorocarbon (PPFC). The specific advantages and disadvantages for each potential low k ILD material were evaluated. It was discovered that highly energetic deposition processes are required for the formation of thermally and environmentally stable carbon or boron nitride ceramics, and the resulting films may have many potentially valuable applications, such as diffusion barriers, tribological coatings, micro-sensor materials, etc. The films are not suitable as low k ILDs, however, because the highly energetic deposition process leads to films with high atomic density, and this leads to high dielectric constants. SiOF shows promise as a low k ILD material for near-term applications, but special passivation or encapsulation strategies may be required in order to reduce two instability problems that we have discovered: moisture absorption and thermal instability of the SiOF/Al interface. PPFC films offer promise for even lower dielectric constant ILDs than SiOF, but it will be necessary to develop new strategies to passivate the free radicals in the films generated during deposition. These free radicals lead to increase in dielectric loss over time when the films are exposed to room ambient conditions.

Acknowledgments

Numerous people made valuable technical contributions to the work discussed in this project. For the synthesis and characterization of the novel dielectric materials we would like to thank C. A. Apblett (Motorola Corp., Austin, TX), J. C. Barbour (Sandia, NM), R. J. Buss (Sandia, NM), D. R. Denison (Lam Research Corp., Fremont, CA), S. C. Fleming (Univ. of Texas, Austin, TX), T. A. Friedmann (Sandia, NM), K. F. McCarty (Sandia, CA), and P. B. Mirkarimi (Lawrence Livermore National Lab, CA). For additional characterization of these materials and/or assistance in the processing of these materials, we would like to thank A. G. Baca (Sandia, NM), W. R. Bayless (Sandia, NM, retired), G. Copeland (Sandia, NM), F. Dominguez (Sandia, NM, retired), R. G. Dunn (Sandia, NM), S. R. Kurtz (Sandia, NM), M. L. Lovejoy (Sandia, NM), L. J. Martinez-Miranda (Univ. of Maryland, College Park, MD), J. Mikkalson (Sandia, NM), N. Missert (Sandia, NM), R. R. Padilla (Sandia, NM), P. P. Provencio (Sandia, NM), D. R. Rieger (Sandia, NM), R. R. Rye (Sandia, NM, retired), C. H. Seager (Sandia, NM), M. P. Siegal (Sandia, NM), R. L. Simpson (Sandia, NM), D. R. Tallant (Sandia, NM), and E. L. Venturini (Sandia, NM).

Contents

Figures

Tables

Novel Low Permittivity Dielectrics for Si-Based Microelectronics

I. Introduction

As the operating frequency of current microelectronic devices increases, the need to develop new low permittivity interlevel dielectrics becomes increasingly important. The present situation represents a departure from the previous design rules regarding the limits to device operating frequencies. In the past, the primary factor limiting device operating frequency in Si-based complementary metal-oxide-semiconductor (CMOS) devices was the carrier transit time in the channel of the MOS transistor. The reason for this is intuitively obvious. For carrier transit lengths exceeding the mean scattering length (approximately 100 Å), the carrier transit time is linearly proportional to the channel length. Decreasing the channel length (which typically coincides with reductions in the device minimum linewidth) leads to approximate linear increases in device operating frequency. Problems occur, however, when the transistors are connected together over large distances and high operating frequencies (a few hundred MHz) are employed, as is frequently encountered in conventional microprocessor designs. Under these conditions, the long length of metal interconnect surrounded by dielectric behaves like an RC circuit in series with the individual transistors. As in a conventional RC circuit, the voltage on the interconnect cannot be switched instantaneously – there is a time delay which is characterized by the product of the interconnect resistance and circuit capacitance (the RC time constant). For large area devices operated at very high speeds, this RC delay may be the dominant factor in determining operating frequency.

There are two straightforward approaches to reducing the RC delay: reducing the resistance of the interconnect or reducing the capacitance of the surrounding dielectric. Due to geometry constraints, the only practical approach to achieving these reductions is to change either the interconnect material, the dielectric material, or both. Al, doped with Si and Cu, is the current standard interconnect, and SiO_2, typically deposited by a plasma-enhanced CVD (PECVD) process, is the current standard interlevel dielectric. Since Al is already a low resistivity material, there is little margin for reducing resistivities further. One popular alternative – still in the development stage – is Cu. Replacement of Al by Cu would yield, at best, an approximate 30% reduction in resistivity. The situation for interlevel (or, equivalently, intermetal) dielectrics, ILDs (or IMDs), is considerably brighter. The dielectric constant for SiO_2 ILD films is 3.9. Several potential new dielectric materials exist with dielectric constants near 2, representing a 50% reduction in capacitance. An added benefit of switching to new low dielectric constant (or "low k") dielectrics is that low k dielectrics reduce the drive power required to operate transistors in an ultra-large scale integration (ULSI) circuit. The required drive power scales as CV^2, where C is the capacitance of the circuit, and V is the drive voltage. It should be noted that this benefit is not gained when the Al interconnect is merely replaced with Cu. Figure 1.1 shows the drive power per gate and time delay for three interconnect technologies. For comparison, if a 1 Volt design rule is assumed, it is clear that there is enhanced benefit to replacing the ILD over replacing the interconnect metal. Replacing the ILD leads to larger reductions both in time delay and drive power. Finally, there is a third advantage to switching to a low k ILD: as the density of

interconnect lines increases, there is greater cross-talk (i.e. induced signals from one line to another), but this cross-talk can be reduced by switching to a low k ILD.

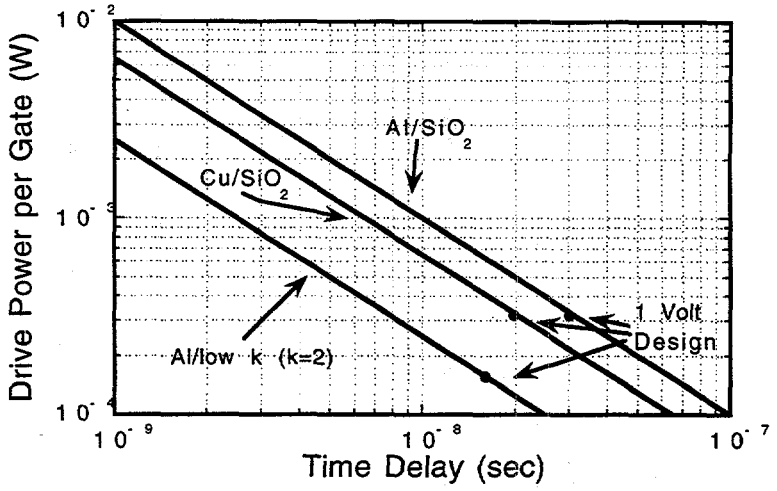

Fig. 1.1. Comparison of drive power per gate and time delay for three interconnect technologies. Switching to a low k dielectric reduces both time delay and required drive power.

The minimum requirement of any new low k dielectric is, of course, that the material exhibit a low dielectric constant (low electrical permittivity). For most solid state materials, there can be up to three contributions to the electrical permittivity: orientational polarizability, molecular or ionic polarizability, and electronic polarizability. Orientational polarizability arises from the re-orientation of polar groups; molecular or ionic polarizability arises from the displacement of ions or polar molecular species; and electronic polarizability arises from polarization of the electronic charge density around atomic cores. Each of these contributions to the electrical permittivity has a characteristic frequency range over which the polarized unit may respond to an applied time-varying field: the cut-off frequency for orientational polarization is in the RF range, for molecular or ionic polarizability it is in the microwave range, and for electronic polarizability it is in the optical range. Figure 1.2 summarizes the three contributions to electrical permittivity and their characteristic frequency ranges. Since the operating frequencies for most ULSI circuits are on the order of 100 MHz, the molecular and electronic polarizabilities are the dominant contributions to the electrical permittivity. Occasionally orientational polarizability may be important if there exists small polar units with low activation barriers for re-orientation, such as unbound water molecules. By considering the contributions to the electrical permittivity, it can be stated that the optimal materials should have no polar groups which can re-orient, the ionic or molecular units should be rigidly fixed to their equilibrium positions, and the electronic charge density should be compact and non-diffuse. Ideally, the solid should consist of a single element arranged in a space group in which every site is identical. In this case there are no polar bonds, and only the electronic contribution to the polarizability applies. This idealized situation is attained by probably only one dielectric material, crystalline diamond. Even so, the dielectric constant of crystalline diamond is

5.7, which is greater than that of SiO_2 films, 3.9. The reason for this apparent dilemma is strikingly simple. The bulk polarizability of a material is a sum of local polarizabilities. Decreasing the number of polarizable units (i.e. decreasing the atomic density of the material) is often the *single most important factor* leading to a low k material. In some cases, the density of the material is determined not by thermodynamics, but rather by the kinetics of the deposition process. This is particularly true for thin films which are often deposited far from equilibrium. Therefore, care should always be taken when describing some new low k material, for the deposition procedure used to create the material may be as significant in influencing the dielectric constant than the intrinsic polarizability of the material itself.

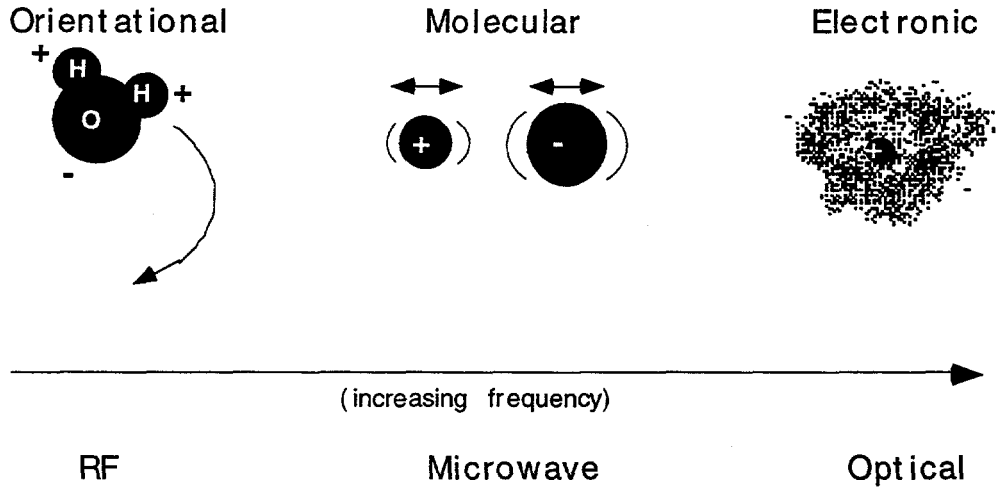

Fig. 1.2. The three contributions to the electrical permittivity for solid state materials and the frequency range up to which they apply.

While the existence of a low dielectric constant is a critical requirement for any new low k dielectric material, it is far from being the only requirement. For example, it is equally important that the new material be chemically compatible with Si microelectronics processing. This requirement is extremely stringent. In a typical device fabrication facility the list of approved elements only includes H, B, C, N, O, F, Al, Si, P, Ti, As, W, and, possibly, Co, Cu, and Ta. The creation of a new low k material containing any other element than that on the list would face a sizable challenge for meeting approval. A low dielectric constant and chemical compatibility are, again, far from sufficient for meeting the requirements of a new low k material. An approximately complete list of the requirements is shown in Table 1.1. It should be clear from the table that much development work is required for almost any new proposed dielectric before that material would be able to meet acceptance.

Table 1.1. List of requirements for new low k interlevel dielectrics.

1. Dielectric constant < 3.9
2. Chemical compatibility with Si
3. Highly insulating
4. Good thermal stability (up to 400°C)
5. High resistance to environmental degradation

6. Low hydrogen/moisture content
7. Compatibility with planarization, lithographic, and etching processes
8. Low diffusivity for metallic impurities
9. High breakdown voltage
10. Low dissipation factor
11. Compositional uniformity
12. Low void/crack/defect density
13. Low compressive stress
14. Conformal deposition
15. Good adhesion
16. Low deposition temperature
17. Thickness uniformity over large areas
18. Low particle density
19. High elastic modulus
20. Low shrinkage
21. Low thermal expansion

In this research program, we have focused on three classes of low k dielectric materials: (1) novel covalently-bonded ceramic dielectrics, (2) fluorinated SiO_2 films, and (3) plasma polymerized fluorocarbon materials. (1) The covalently-bonded ceramic dielectrics include materials comprised of carbon, boron, and/or nitrogen, all of which are compatible with Si. These materials exhibit unique properties and some promise for exhibiting low dielectric constants due to their strong covalent bonding and low molecular weight. (2) Fluorinated SiO_2 films have previously been shown to exhibit dielectric constants in the range of 3.5. In this report we focus on some special challenges regarding the stability of these materials. (3) Plasma polymerized fluorocarbons exhibit great promise for achieving low dielectric constants using a deposition process which is readily compatible with ILD fabrication. As discussed in this report, there are technical problems with these materials which need to be solved, however. Finally, there were a number of low k dielectric materials that fell outside the scope of this program. These include materials such as fluorinated silsesquioxanes, aerogels (highly porous SiO_2), and numerous fluorinated long-chain polymers, including fluorinated polyimides, fluorinated poly(arylethers), etc. Research on most of these other materials is either currently supported by other research programs or is under the direction of commercial enterprises.

II. Covalently-bonded Ceramics: Amorphous Carbon and Boron Nitride†

Insulators formed from first-row elements are good candidates for low permittivity dielectrics, with their bulk dielectric constants in the range ~ 5 to 8 for such materials as BeO, cubic BN (c-BN), and diamond.[1] Insulating films of carbon and BN are especially promising due to their compatibility with Si processing. Most studies have concentrated on chemical vapor or plasma-enhanced chemical vapor deposition (CVD and PECVD) which leads to insulating diamond-like carbon, DLC, films (films of amorphous carbon containing hydrogen) and films of predominantly hexagonal BN, h-BN. There have been numerous reports of the dielectric constants of these materials being less than or approaching that of SiO_2 (see Table 2.1).[2-11]

Table 2.1. Reported dielectric constants for DLC and BN films.

Film	Dielectric Constant	Deposition	Ref.
DLC	3.9	PECVD	2
DLC	4.2	PECVD	3
DLC	4.5	PECVD	4
DLC	< 4	PECVD	5
h-BN	4.0-4.7	PECVD	6
h-BN	2.2-4.41	PECVD	7
h-BN	2.9	PECVD	8
h-BN	2.9-4.3	PECVD	9
h-BN	3.3-3.5	CVD	10
h-BN	3.7	CVD	11

Despite the low dielectric constants, these films are not suitable as interlevel dielectrics due to thermal or environmental degradation. At temperatures above ~ 300°C, hydrogen comes out of DLC resulting in the transformation of C-C:H sp^3 bonds to C-C sp^2 bonds, as evidenced by changes in the Raman spectra and increased optical absorption.[12] This leads to non-insulating films which are unsuitable as an interlevel dielectric. h-BN films are hygroscopic, rapidly deteriorating under conditions of high humidity.[8,11] These deficiencies can be overcome by depositing insulating carbon films free of hydrogen, called amorphous tetrahedrally-coordinated carbon (a-tC) and by depositing cubic BN (c-BN) films. a-tC films are stable – as indicated by Raman – at temperatures up to ~ 800°C in inert ambients,[13] while c-BN is an environmentally stable bulk ceramic. The dielectric characteristics of these films are discussed below.

The a-tC films were deposited using PLD in high vacuum (10^{-8} - 10^{-7} Torr) with a KrF laser and a rotating graphite target . For some depositions, a background gas of H_2 or N_2 (10 mTorr) was also used. The energy density of the laser light focused onto the rotating graphite target was adjusted between 5 to 48 J/cm^2 leading to films with a varying degree of sp^3 bonding. In all cases, deposition was performed at *room temperature* with no subsequent annealing.

The formation of c-BN films is difficult. Although there have been reports of the formation of c-BN using PECVD techniques,[14] the volume fraction of c-BN material is lower than that

demonstrated for c-BN films prepared by PLD.[15] In this work, the c-BN films were deposited using ion-assisted PLD in high vacuum with a KrF laser, a rotating h-BN target, and a broad-beam Kaufman-type ion source. The typical deposition conditions leading to c-BN material were as follows: laser energy density=4 J/cm^2, ion beam gas mix=60% N_2/40% Ar, ion energy=1000 eV, ion current=450 μA/cm^2, and substrate temperature=400°C. Under these conditions, the films contained greater than 85% c-BN with the balance h-BN, as determined by Fourier Transform Infrared (FTIR) Spectroscopy (by h-BN here, and in references below, we refer to all sp^2-bonded phases of BN, including turbostratic BN and amorphous BN). The stoichiometry of the films was verified by Rutherford Backscattering Spectroscopy (RBS) and Elastic Recoil Detection (ERD) and was found to be B:N = 1:1 within experimental accuracy.[15]

Additionally, h-BN films were deposited by PLD (as above, except under conditions which favor h-BN formation – lower ion fluxes, lower deposition temperatures, etc.) and by ECR deposition. The typical conditions for ECR deposition were 1400W RF power, 70% N_2/30% B_2H_6, and a substrate temperature of 260°C. h-BN films prepared in this way showed negligible c-BN content as measured by FTIR.

For dielectric characterization, the a-tC films were deposited on heavily-doped (~ 0.01 Ωcm) n- and p-type Si substrates as well as on substrates containing a layer of TiW or TiN (~ 2000 Å) atop a thick layer of SiO_2 (~ 1 μm) on Si. Due to poor adhesion to the metal films, the c-BN and h-BN films were only deposited on heavily-doped to moderately-doped (0.01 Ωcm and 0.1 to 30 Ωcm) p-type Si. Square and circular Ti-Au or Al contacts were made to the dielectric films either by photolithography and lift-off or by metal evaporation through a shadow mask. Diode sizes defined lithographically ranged from 50 μm to 400 μm, while those defined by shadow mask ranged from ~ 127 μm to 1270 μm. Actual diode sizes were verified by optical microscopy. Backside contacts were made to the p-type wafers by an In-Ga eutectic alloy and to the n-type wafers by heat-diffused Sb, followed by the In-Ga eutectic. Typical film thicknesses for the a-tC and c-BN films were 1000 Å, while the ECR deposited h-BN films were thicker, ~ 1 μm. Film thicknesses were measured by profilometry and, on select samples, were corroborated by ellipsometry, transmission electron microscopy, or x-ray reflectivity. Uncertainties in the measured film thicknesses are estimated to be up to 10%, leading to uncertainties in the measured dielectric constants of up to 10%.

Current-voltage (IV) and capacitance-voltage (CV) characterization were performed on the metal-insulator-metal (MIM) and metal-insulator-semiconductor (MIS) diodes at frequencies ranging from 20 kHz to 4 MHz. The IV and CV measurements were performed for a variety of diode sizes to verify geometric scaling. Capacitances and AC conductances for the MIM diodes were typically found to vary by less than 5% over the frequency range 20 kHz to 4 MHz, indicating negligible influence of any short time constant trap states in the bulk of the dielectric. The insulator capacitance was determined from the MIS diodes by biasing the device towards accumulation. Typically, a test frequency of 1 MHz was employed to reduce the contribution of any fast interface states.

A. Evaluation of a-tC

The dielectric characteristics of a-tC films depend greatly on the deposition conditions, particularly the laser energy density impinging on the graphite target. The measured resistivities from MIM diodes for a-tC films (measured normal to the plane of the film) are shown as a function of diode size and laser energy density in Fig. 2.1. Each data point represents the median resistivity measured from several diodes. At the smallest diode sizes there is a monotonic decrease in resistivity with decreasing laser energy density, while this trend disappears at the larger diode sizes (the apparent increase in resistivity in the 5.3 J/cm^2 sample is likely due to conduction paths extending beyond the periphery of the diode – an edge effect). Films deposited at 45 J/cm^2 in 10 mTorr ambients of H_2 or N_2 showed resistivities > 10^6 Ωcm and less than 100 Ωcm, respectively. Sheet resistance measurements performed for the 48 J/cm^2 and 19 J/cm^2 a-tC films on insulating substrates uniformly show high resistivities, > 10^6 Ωcm, suggesting that the resistivity drop at larger diode sizes and the low resistivities in the samples deposited at low energy density are due to low resistivity shorts between the top and bottom electrodes in the film. Scanning electron microscopy did not find pinholes or particles in the films at the densities necessary to explain the electrical shorting in the film. On the other hand, optical absorption at visible and IR wavelengths was found to increase with decreasing energy density, strong C-C stretching modes characteristic of 3-fold coordinated sp^2-bonded carbon were observed by Raman spectroscopy, and transmission electron energy loss spectroscopy showed increased π-bonded carbon at low laser energy densities, suggesting that one possible source of shorts may be 3-fold coordinated, conducting regions in the a-tC material. For dielectric characterization, only the most resistive a-tC films deposited at the highest laser energy densities were considered.

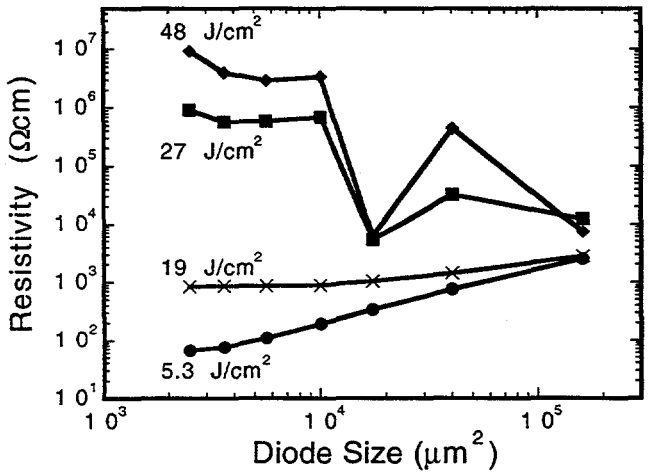

Fig. 2.1. Median resistivities of a-tC films measured from MIM structures.

The measured dielectric constants of a-tC films, determined from MIM structures with TiW, as a function of laser energy density are shown in Fig. 2.2. Characteristics of a sample grown in 10 mTorr H_2 are also shown. In all cases the normal film resistivities exceeded 10^6 Ωcm, and the phase angle of the measured admittance was close to -90°. The solid circles indicate the mean of several measurements on one or two different samples at each deposition condition. The error bars reflect the total variation in measured dielectric constants for a particular sample deposition condition, not the error associated with each measurement of the dielectric constant (which is on the order of 10%, due to thickness uncertainty, as discussed above). For samples deposited in vacuum, the dielectric constant is essentially independent of laser energy density and falls within the range of 5 to 8, typically being close to 6.5. Surprisingly, the sample deposited in an ambient of H_2 exhibits a dielectric constant exceeding 8. It might be expected that a-tC films deposited in H_2 ambients – which show Raman features similar to that of DLC – would show dielectric constants similar to that of DLC (about 4.0, see Table 2.1). In contrast to the role of hydrogen in (PE)CVD deposition of DLC, a H_2 gas ambient used with the PLD of carbon produces two effects: it results in the attenuation of the energies of the carbon species in the laser ablation plume, leading to the production of material with higher sp^2 content – similar to the a-tC material deposited at lower laser energy densities; and, secondly, hydrogen bonds to the trigonally-coordinated carbon, stabilizing the bonding into 4-fold coordination. Apparently the degree of hydrogen saturation of sp^2 bonds in the a-tC material may not be as complete as that of DLC material (which is grown from a hydrogen containing precursor) and conductive regions of sp^2 material may be present in the sample, thus contributing to higher apparent dielectric constants.

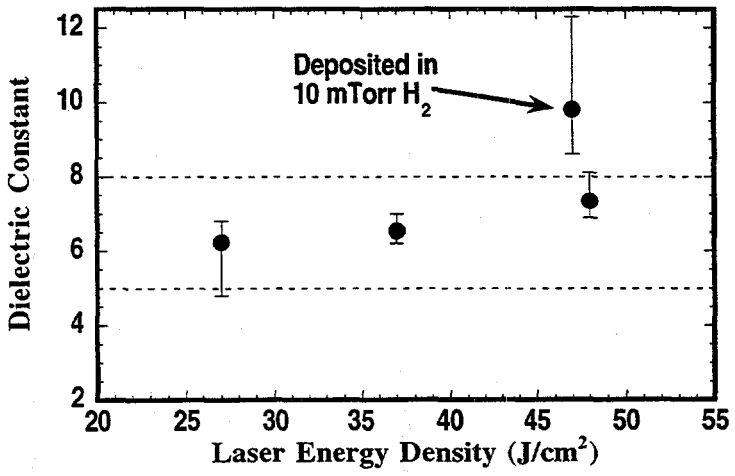

Fig. 2.2. Measured dielectric constants for a-tC films deposited in vacuum and hydrogen as a function of aser energy density.

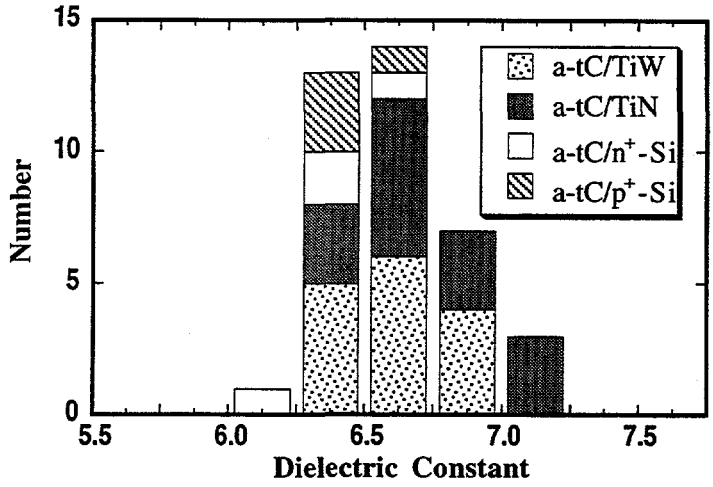

Fig. 2.3. Histogram of measured dielectric constants or a-tC MIM and MIS diodes.

B. Evaluation of BN

The c-BN and h-BN films deposited by PLD are highly resistive, with resistivities deduced from MIS structures approaching 10^{14} Ωcm. Typical capacitance-voltage (CV) scans for MIS diodes on one c-BN sample are shown in Fig. 2.4. Modulation in the CV was observed suggesting some movement in the Fermi level at the c-BN/Si interface, but the curves show stretch-out and a slight flat-band voltage shift indicating a high density of interface states, potentially depressing the capacitance maximum. As a result, the permittivities extracted from the measured insulator capacitance, C_i, provide a lower bound for the true film permittivities.

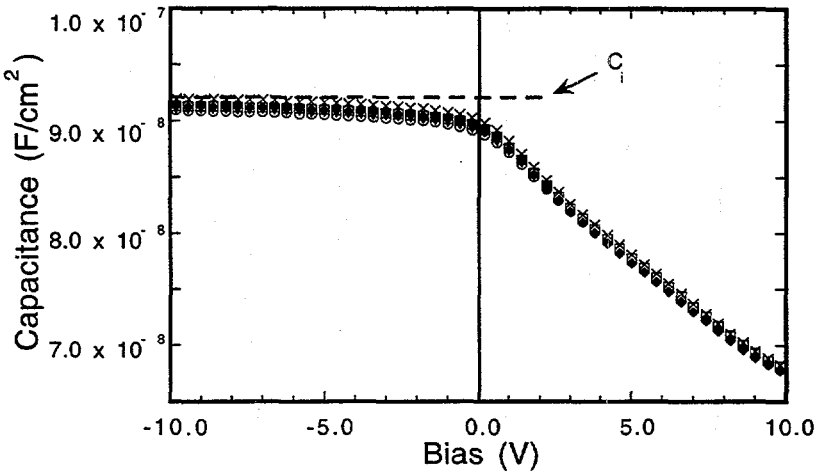

Fig. 2.4. CV curves for c-BN MIS diodes measured at 1 MHz. The insulator capacitance is measured from the saturated value of the accumulation capacitance.

Fig. 2.5 is a histogram of the dielectric constants measured from MIS diodes with PLD c-BN and h-BN layers and ECR deposited h-BN layers. Two or more separate samples were measured from each group. The c-BN samples exhibited the highest dielectric constants of around 7.5, the PLD h-BN samples were clustered around 5.5, and there was one group of ECR h-BN samples less than 4.0 with the other group around 5.5. Although the deposition conditions for the ECR h-BN samples were nominally identical, the measurements were performed at different places on the substrate, with the low dielectric constant measurements being made near the center of the wafer and the higher dielectric constant measurements being made near the edge (presumably somewhat removed from the main focus of the ECR flux).

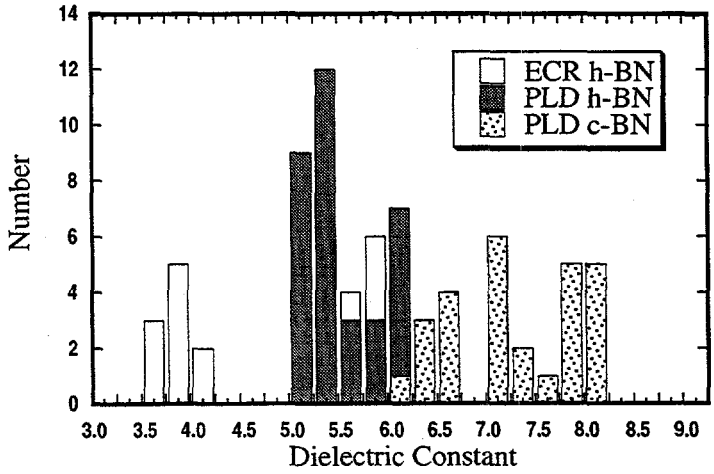

Fig. 2.5. Histogram of dielectric constants of BN films.

C. Discussion of dielectric properties

Table 2.2 summarizes the average dielectric constants measured for the PLD a-tC and BN films and the ECR BN films along with the dielectric constants of bulk diamond and BN. The dielectric constants for the PLD films are both higher than the (PE)CVD film equivalents and are comparable to the bulk values. These two results may be readily understood upon examining the characteristics of the PLD process and the resulting films. The deposition rate for PLD tends to be slower than that of (PE)CVD, about 0.3 μm/hr compared to the ECR process of 5 μm/hr for the films discussed here. In addition to the slower growth rate, PLD is an energetic process in which neutral species with energies of the order of 10 eV and ions with energies of the order of 100 eV form the deposit. These energies are high enough that subsurface growth (i.e. implantation) occurs. Finally, as discussed earlier, the PLD process can be performed in vacuum ambients where there is little opportunity for background gas or reaction species (CH_x, for example) to be incorporated into the growing film. These characteristics all contribute to the formation of films with higher densities than their (PE)CVD counterparts. The densities of a-tC films deposited with a laser energy density of 45 J/cm^2 have been measured by x-ray critical angle reflectivity and were found to be over 3.0 g/cm^3.[16] This is less than the density of crystalline diamond, about 3.5 g/cm^3, but is approximately 50% denser than typical DLC films (densities around 1.7-2.3 g/cm^3, which is comparable to that of graphite, 2.2 g/cm^3).[17] The influence of a-tC film density on measured film permittivities is shown in Fig. 2.6. The observation that the dielectric constants of a-tC films exceeds that of crystalline diamond despite the lower densities for a-tC is an indication of heterogeneity in the structure of a-tC. As a simple approximation, if we assume the internal structure of a-tC is described by the presence of conductive spheres (e.g. 3-fold regions) in an insulating matrix (4-fold regions), then the permittivity enhancement is adequately described by the Maxwell-Wagner effect.[18] The observed dielectric constant for a-tC films shows no dispersion over the frequency range ~70 kHz to 4 MHz. This is not inconsistent with a heterogeneous dielectric. Again, assuming a simple Maxwell-Wagner model, no strong dispersion is expected until the measurement frequency exceeds several GHz, see Fig. 2.7. In actuality the a-tC material cannot be simply described by a system of conductive spheres in an insulating matrix. Most theoretical models indicate that the 3-fold regions do not cluster, rather than link into chain-like structures with fractal dimension between 1 and 2.[19] The electronic transport in this system is governed by hopping conduction along the chain-like structures combined with chain to chain tunneling.[20,21]

Table 2.2. Measured dielectric constants of a-tC and BN films.

Material	Dielectric Constant
a-tC	~ 6.5
Bulk Diamond	5.7
PLD c-BN	6.5-8.0
Bulk c-BN	7.1
PLD h-BN	5.0 -6.0
ECR h-BN #1	~ 3.75
ECR h-BN #2	~ 5.75
Bulk h-BN	~ 5.7

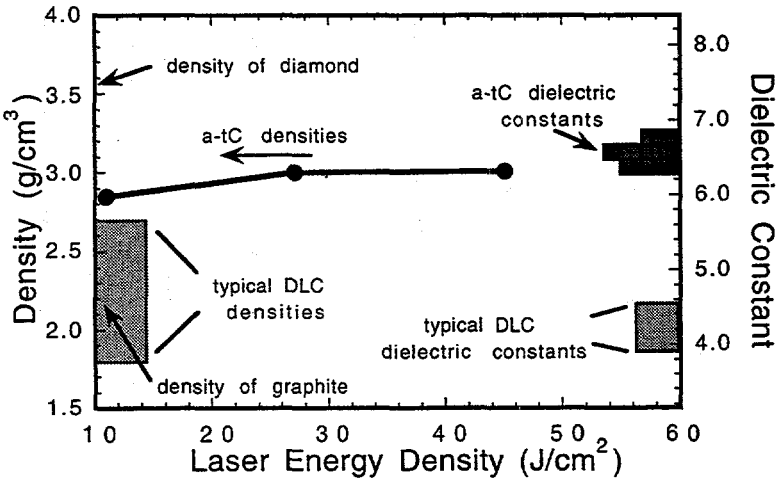

Fig. 2.6. Correlation of film density and dielectric constants for a-tC and DLC films.

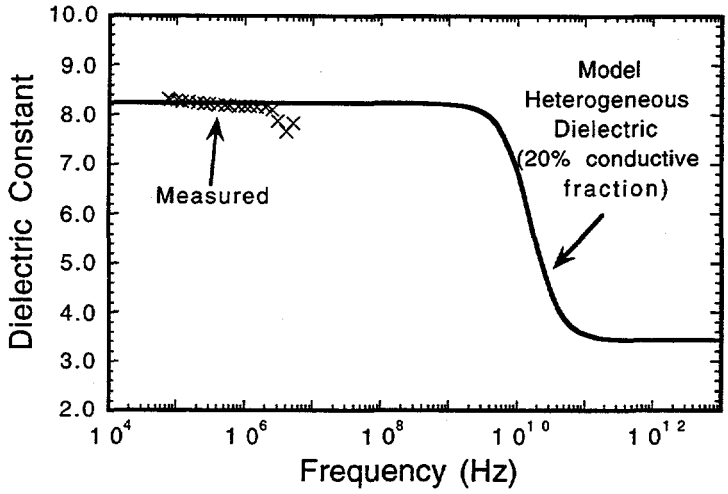

Fig. 2.7. Measured and simulated dispersion of the dielectric constant for an a-tC film. The model assumes a film with 20% volume fraction of conductive spheres in an insulating matrix.

The situation for BN films is very similar to that for a-tC. Measured densities for the PLD films are similar to the bulk densities of h-BN and c-BN, while the measured densities for the ECR films are up to 50% less (in the range of 2.4 g/cm^3). This density difference is sufficient to explain the observed variation in dielectric constants. The reason for the large difference in dielectric constants for the ECR films (prepared identically, but measured at different points on the wafer) is not well understood; differences in film density or potential non-stoichiometry in the film near the edge of the wafer may be playing a role.

The requirements of thermally and environmentally stable carbon-based or BN films for microelectronics and the need for low permittivities may be fundamentally conflicting. It is the addition of hydrogen to sp^2-bonded carbon which enables the formation of sp^3-bonded carbon. In order to create sp^3-bonded carbon films in the absence of hydrogen, high internal compressive stresses (hence, high atomic densities) may be required – at least during film deposition – to promote the formation of sp^3 bonds over sp^2 bonds.[22] Hence, thermally stable, hydrogen-free carbon films may always coexist with higher permittivities. The formation of c-BN over h-BN may also require high internal stresses/atomic densities; thus, leading to higher permittivities. Therefore, attempts to combat environmental degradation in PECVD BN films via the formation of c-BN while maintaining low permittivities may be ineffective. Because of the high permittivities, applications for hydrogen-free DLC or c-BN films should take advantage of their high thermal and environmental stabilities, e.g. application as thin encapsulants or diffusion barriers. Indeed, the potential of DLC as an encapsulant has already been discussed.[23]

The dielectric behavior of a-tC and BN films can be summarized succinctly: the observation of low dielectric constants for carbon and BN films deposited by PECVD processes is a result of low film densities. When the films are deposited by non-CVD, energetic processes which lead to

dense, bulk-like film densities, the observed dielectric constants are, as expected, bulk-like. The enhanced film density for these non-CVD processes improves the film's resistance to thermal and environmental degradation. There may be microelectronic applications (e.g. diffusion barriers) which could benefit from such films.

†In collaboration with T. A. Friedmann, C. A. Apblett, P. B. Mirkarimi, K. F. McCarty, M. P. Siegal, N. Missert, and M. L. Lovejoy.

References

1. Landolt-Börnstein: Numerical Data and Functional Relationships in Science and Technology, edited by O. Madelung, M. Schulz, and H. Weiss (Springer-Verlag, Berlin, 1982).
2. A. Ishii, S. Amadatsu, S. Minomo, M. Taniguchi, M. Sugiyo, and T. Kobayashi, J. Vac. Sci. Technol. A **12**, 1068 (1994).
3. T. Mandel, M. Frischholz, R. Helbig, and A. Hammerschmidt, Appl. Phys. Lett. **64**, 3637 (1994).
4. Th. Mandel, M. Frischholz, R. Helbig, S. Birkle, and A. Hammerschmidt, Appl. Surf. Sci. **65/66**, 795 (1993).
5. K. K. Chan, S. R. P. Silva, and G. A. J. Amaratunga, Thin Solid Films **212**, 232 (1992).
6. S.V. Nguyen, T. Nguyen, H. Treichel, and O. Spindler, J. Electrochem. Soc. **141**, 1633 (1994).
7. D. C. Cameron, M. Z. Karim, and M. S. J. Hashmi, Thin Solid Films **236**, 96 (1993).
8. M. Maeda, T. Makino, E. Yamamoto, and S. Konaka, IEEE Trans. Electron Devices **36**, 1610 (1989).
9. W. Schmollla and H. L. Hartnagel, Solid State Electron. **26**, 931 (1983).
10. M. Hirayama and K. Shohno, J. Electrochem. Soc. **122**, 1671 (1975).
11. M. J. Rand and J. F. Roberts, J. Electrochem. Soc. **115**, 423 (1968).
12. J. E. Parmeter, D. R. Tallant, and M. P. Siegal, Mat. Res. Soc. Proc. **349**, 513 (1994); D. R. Tallant, J. E. Parmeter, M. P. Siegal, and R. L. Simpson, Diamond Relat. Mater. **4**, 191 (1995).
13. M. P. Siegal, T. A. Friedmann, S. R. Kurtz, D. R. Tallant, R. L. Simpson, F. Dominguez, and K. F. McCarty, Mat. Res. Soc. Proc. **349**, 507 (1994); and T. A. Friedmann, K. F. McCarty, and M. P. Siegal, in preparation.
14. S. Y. Shapoval, V. T. Petrashov, O. A. Popov, A. O. Westner, M. D. Yoder, Jr., and C. K. C. Lok, Appl. Phys. Lett. **57**, 1885 (1990).
15. T. A. Friedmann, P. B. Mirkarimi, D. L. Medlin, K. F. McCarty, E. J. Klaus, D. R. Boehme, H. A. Johnsen, M. J. Mills, D. K. Ottesen, and J. C. Barbour, J. Appl. Phys. **76**, 3088 (1994).
16. L. J. Martínez-Miranda, J. P. Sullivan, T. A. Friedmann, M. P. Siegal, T. W. Mercer, and N. J. DiNardo, Mat. Res. Soc. Proc. (1995), in press.
17. M. F. Toney and S. Brennan, J. Appl. Phys. **66**, 1861 (1989); and C. A. Lucas, T. D. Nguyen, and J. B. Kortright, Appl. Phys. Lett. **59**, 2101 (1991).
18. B. K. P. Scaife, *Principles of Dielectrics* (Clarendon, Oxford, 1989).
19. N. A. Marks, D. R. McKenzie, B. A. Pailthorpe, M. Bernasconi, and M. Parrinello, Phys. Rev. Lett. **76**, 768 (1996).
20. J. P. Sullivan, T. A. Friedmann, and A. G. Baca, to appear in J. Electronic Mater., 1997.
21. J. P. Sullivan, to be published.
22. D. R. McKenzie, D. Muller, and B. A. Pailthorpe, Phys. Rev. Lett. **67**, 773 (1991).
23. J. F. McDonald, S. Dabral, X.-M. Wu, A. Martin, and T.-M. Lu, Proc. VLSI Multilevel Interconnect. Conf., 366 (1989).

III. Covalently-bonded Ceramics: Boron-Carbon-Nitrogen Ternaries†

To explore the possibility of synthesizing a new low k dielectric composed of B, C, N – all of which are compatible with Si processing – a materials research effort was initiated. The known bonding and properties of compounds comprised from the first-row elements B, C, and N show tremendous variability – ranging from metallic, layered, 3-fold coordinated graphite to highly insulating, tetrahedrally-coordinated diamond and cubic boron nitride (c-BN), to the semiconducting boron carbides which are distinguished by their icosahedral-based crystal structures. Of these materials, ternary alloys and compounds of boron-carbon-nitrogen (BCN) have received much recent interest for their potential applications as ultra-hard materials,[1] electrodes for electrochemical cells[2], or highly-efficient cold cathode electron emitters.[3] Considerable theoretical[4,5] and experimental[6-11] work has been performed to understand the bonding, properties, and fabrication of these materials. One issue which has remained is the nature of the local atomic bonding in these materials. Recent experimental work has contributed to the development of two differing views: one of local phase segregation into graphite and hexagonal BN (h-BN)[7] and the other of local intermixing of the three elements.[6] Since most experimental evidence suggests that BCN compounds are thermodynamically unstable with respect to dissociation into carbon and BN,[9] routes to achieving true atomically-mixed phases of BCN must rely on deposition or growth processes far from equilibrium. In this work, we have focused on the deposition of BCN thin films using pulsed-laser deposition (PLD). PLD has been successfully used in the past to deposit metastable materials under conditions in which bulk synthesis under equilibrium conditions could not occur, e.g. the deposition of c-BN at temperatures < 400°C.[12] To gain insight on local bonding in BCN materials we have investigated the structural and bonding properties of these films using transmission electron microscopy, Fourier transform infrared spectroscopy, Raman spectroscopy, and electrical measurements. We have also measured the field emission properties of these materials to assess recent claims of superlative electron emission properties for BCN films.[3]

The thin films of BCN were deposited using PLD with a KrF (248 nm) laser focused to an energy density over 40 J/cm^2 on to a rotating solid target of either B_4C (Cerac Inc., 99.5% purity) or a mixed target consisting of 2/3 pyrolytic graphite and 1/3 pyrolytic h-BN. Typical film thicknesses ranged from ~ 60 - 130 nm. Deposition was performed on either Si substrates or metallized Si substrates consisting of W(200 nm)/SiO_2(1000 nm)/Si. The substrate temperature was varied from room temperature to 500°C by either resistive heating of the substrate (for Si substrates) or thermal contact with a resistively heated substrate (for the metallized Si substrates). For all of the BCN samples deposited by PLD from the B_4C target and for some of the samples deposited by PLD from the graphite/h-BN target, additional nitrogen was supplied to the film using a broad-beam Kaufman-type ion source. Both pure N_2 beams and mixed N_2/Ar beams were used with beam voltages ranging from 200 to 800 V and ion fluences on the substrate, assuming single ionization, ranging from ~ 3 x 10^{14} cm^{-2}sec^{-1} to ~ 10^{15} cm^{-2}sec^{-1}. For comparison, the average fluence of B, C, or N species deposited on to the substrate via laser ablation of the target was ~ 5 x 10^{14} cm^{-2}sec^{-1} (approximate deposition rate of 2.5 nm/min). The chamber background pressure in

the absence of ion irradiation was 10^{-8} Torr and, during ion irradiation, 10^{-4} Torr (all N_2 or N_2/Ar).

Plan-view transmission electron microscopy (TEM) and diffraction (120 keV) was used for structural characterization. The TEM samples were prepared by ultrasonic drilling of 3 mm disks from the sample, mechanical polishing, and chemical etching of a small hole (0.5 -1.0 mm) using $HF/HNO_3/CH_3COOH$. The BCN films showed no evidence of chemical etching and, thus, formed unsupported membranes. Compositions of the deposited BCN compounds were measured using ion beam analysis. The carbon and nitrogen concentrations were measured by Rutherford backscattering (RBS) while the boron concentration was measured using elastic recoil detection (ERD). Both FTIR and Raman spectroscopy were used for vibrational characterization. Electrical characterization was performed on BCN samples deposited on metallized Si substrates. Ti/Au top metal contacts were fabricated by photolithography and lift-off or deposition through a shadow mask. Field emission characterization was performed in a scanning electron microscope (SEM) with base pressure ~ 10^{-7} Torr. Direct electrical connection to the metallized substrate was used for the cathode contact and a 2 mm diameter stainless steel ball suspended 10 - 50 μm above the sample was used as the anode. Following emission characterization, the SEM was used to verify that no damage (e.g. cratering due to electrical discharge) had occurred during testing.

The deposition conditions used in this study led to BCN compounds clustered at three compositions as shown in Fig. 3.1. Ablation of a B_4C target with N ion irradiation led to BCN alloys with compositions falling close to the carbon-deficient end of the BN–C tie line (composition close to $BC_{0.15}N$). Constant ion irradiation conditions of 800 V acceleration, pure N_2, and ion fluences of ~ 4 x 10^{14} $cm^{-2}sec^{-1}$ were used, while the substrate temperature was varied from 100°C to 300°C. The highest N concentration in the BCN alloys occurred for samples deposited at a substrate temperature of 100°C, suggesting that N incorporation in the films decreases at higher deposition temperatures, as is also observed in ion-assisted PLD of AlN.[13] Deposition at temperatures up to 500°C gave similar film properties to those discussed here, and were, thus, not characterized separately in terms of composition.

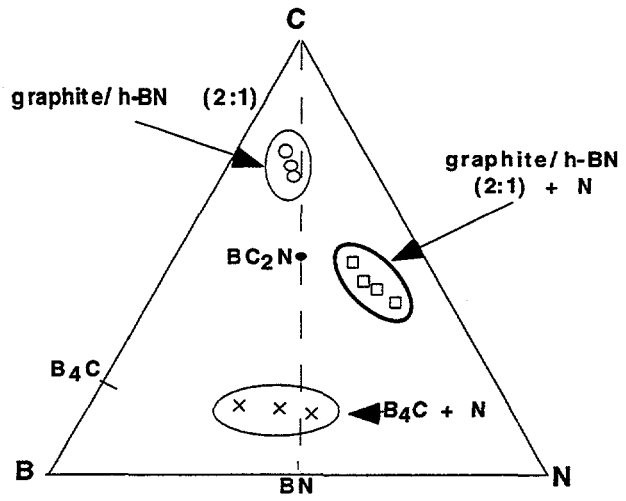

Fig. 3.1. Measured compositions for BCN thin films deposited by PLD using B_4C targets and N ion irradiation or composite graphite/h-BN targets (in a ratio of 2:1) with and without N ion irradiation.

In order to achieve a film composition close to BC_2N, PLD using a composite 2/3 graphite and 1/3 h-BN target was performed. BC_2N is an approximate composition that is readily obtained by chemical vapor deposition (CVD) from acetonitrile and boron trichloride.[10,14] This composition has also received considerable theoretical interest in terms of its potential bonding and electronic structures.[4] The measured compositions of the BCN films using this composite target and substrate temperatures from ~ 25°C to 300°C are shown in Fig. 3.1. The measured compositions are all more carbon-rich (approximate composition close to BC_4N) than the intended composition, BC_2N, and show little sensitivity to substrate temperature (the sample with the lowest carbon concentration was deposited at a substrate temperature of 300°C). The high carbon concentrations (BC_xN, $x > 2$) observed for the deposited films is probably due to an unintentionally high carbon concentration in the ablation target, rather than from a loss of B and N in the film during the ablation process.

Ion-assisted PLD using the composite target was also performed. Ion irradiation conditions of 200 - 800 V acceleration, pure N_2, and ion fluences of ~ 8 x 10^{14} $cm^{-2}sec^{-1}$ were used, while the substrate temperature was varied from ~ 25°C to 300°C. Measured compositions are shown in Fig. 3.1. The sample with the highest N concentration was deposited with 200 V ion acceleration at a substrate temperature of 150°C (higher substrate temperatures, 300°C, and higher accelerating voltages, 800 V, led to lower N concentrations in the film).

The compositions for BCN films deposited using other techniques can also show large ranges. In addition to compositions near BC_2N using CVD with acetonitrile and BCl_3, compositions near B_2C_5N using CVD with BCl_3 and mixtures of acetylene, ammonia, and carrier gases,[15] compositions near $B_{1.0}C_{0.7}N_{0.7}$ using electron cyclotron resonance CVD,[16] and a wide range of compositions using pyrolytic deposition[17] have been observed. This suggests that there is little driving force for line compound formation in this system.

Structural characterization of the BCN films was performed using plan-view TEM and electron diffraction. Electron diffraction for all the films typically showed 4 weak, diffuse rings. Imaging under bright-field conditions indicated little discernible contrast, while dark-field imaging using the innermost ring (indexed as 002) revealed a high density of nanocrystallites with typical dimensions less than 5 nm.

X-ray diffraction was found to be ineffective for structural analysis due to these extremely fine crystallite sizes and small film thicknesses, so electron diffraction analysis was employed. Fig. 3.2 shows measured d-spacings and relative intensities (approximately logarithmic) for the BCN films and related compounds.[18] The dominant peak occurs at an approximate d-spacing of 3.50 Å for BCN films deposited using B_4C targets and N ion irradiation and a d-spacing of 3.38 Å for BCN films deposited using the graphite/h-BN composite target with and without N ion irradiation. The other peaks are generally consistent with the (00l) and (hk0) peaks of turbostratic hexagonally layered compounds of graphite, h-BN, or h-BCN, which strongly suggests the existence of a layered structure to these BCN films. There may be evidence of other phases, however. The strong peak near 2.12 Å observed in the BCN films is also near the dominant (111) peak of cubic BN (c-BN), suggesting a possible contribution from c-BN in the films [it should be noted that dark-field imaging using an aperture centered on this second ring did not reveal a clearly different structure than dark-field imaging centered on the (002) ring, however].

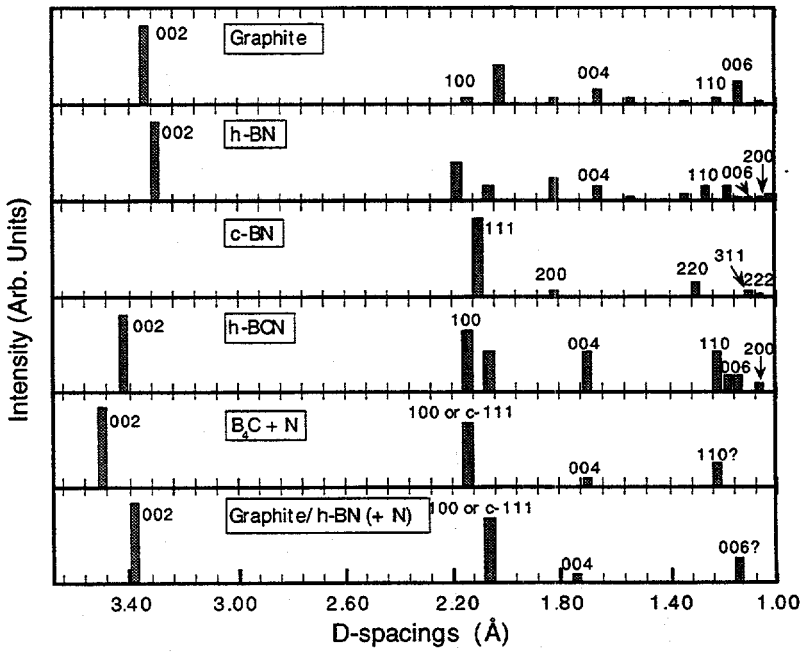

Fig. 3.2. Electron diffraction peak positions and intensities for BCN films (bottom 2 panels) compared to peak positions and x-ray intensities for related compounds (top panels). Approximate logarithmic peak intensities are shown. The suggested assignment of reflections for the peaks in the BCN films is shown.

Some possible evidence for the presence of c-BN may be found in the BCN films' FTIR spectra. Reflectance FTIR of a BCN film deposited from the B_4C target with N irradiation and a substrate temperature of 250°C is shown in Fig. 3.3. Vibrational modes near 800 and 1400 cm^{-1} are similar in peak position and relative intensities as those frequently found for h-BN films, while the vibrational mode near 1100 cm^{-1} is consistent with the presence of c-BN in the film.[12] A c-BN component to the film would not be surprising; c-BN films have been formed under similar deposition conditions using N ion irradiation and ablation from an h-BN target (as opposed to the B_4C target used here).[12] B-C vibrational modes would provide an alternative explanation for the peak near 1100 cm^{-1}, however. Vibrational modes of bulk B_4C are relatively broad but are also peaked near 1080 cm^{-1}.

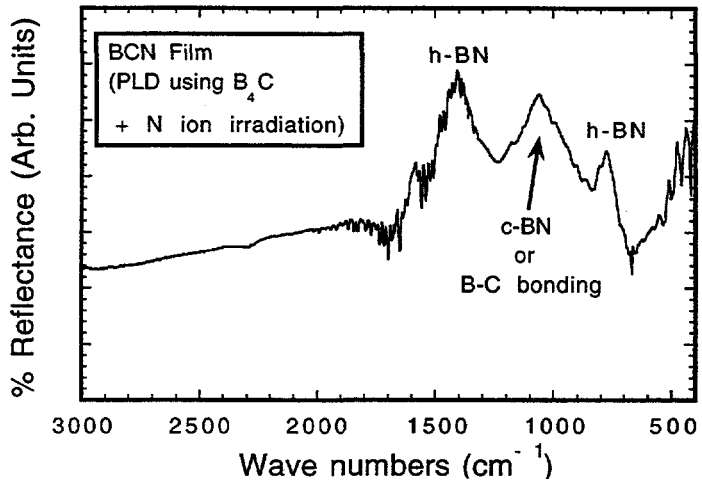

Fig. 3.3. FTIR spectrum of a BCN film prepared by PLD using a B_4C target, N ion irradiation, and a substrate temperature of 250°C. Vibrational bands near 800 and 1400 cm^{-1} likely correspond to h-BN vibrational modes. The band near 1100 cm^{-1} likely corresponds to c-BN, but B-C vibrational modes are also possible.

The peaks near 800, 1100, and 1400 cm^{-1} were present in all of the samples prepared by ablation of the B_4C target, but their relative intensities varied (the 800 and 1400 cm^{-1} peaks always being the most prevalent). These peaks were much less pronounced in films prepared by PLD using the composite graphite/h-BN target. Since these films also contained much lower percentages of B and N, this is, again, consistent with the assignment of these peaks as being BN-related. Both the approximate d-spacings and FTIR spectra observed for the BCN films here are similar to other BCN films deposited by a variety of methods. The measured d-spacings of ~ 3.38 Å and 3.50 Å are in the middle of the range for reported d-spacings for BCN compounds, ~ 3.3 to 3.6 Å.[19] In addition, FTIR spectra which are dominated by BN-like vibrational modes are not uncommon.[16] Given that diffraction, particularly for the nanocrystalline films, is not discriminatory amongst various bonding configurations for B, C, and N and FTIR is not sensitive

to carbon structures in the films (C-C bonds are non-polar and, hence, not FTIR-active) additional characterization is required.

In order to examine the carbon bonding structures in these films Raman spectroscopy was employed. Fig. 3.4 shows a representative Raman spectra for a BCN thin film sample deposited using the composite graphite/h-BN target at a substrate temperature of 300°C with no N ion irradiation. An excitation wavelength of 458 nm was used in order to reduce background fluorescence. This background fluorescence is similar to that observed in pure BN films and is suggestive of the presence of a BN component to the films.[20] It was particularly strong in films deposited using the B_4C target, but was weak in samples deposited using the composite target (which have lower BN concentrations). The Raman spectra in BCN films is dominated by a broad peak near 1200 - 1700 cm^{-1} associated with carbon-related structures and a much weaker peak near 500 - 800 cm^{-1} which is in a range commonly observed for vibrational bands in singly-bonded B, C, and N compounds (see inset of Fig. 3.4). The broad peak near 1200 - 1700 cm^{-1} has a line shape and peak position very similar to that observed for pure carbon films deposited using PLD from graphite at low ($\leq$ 5 J/cm^2) laser energy densities or PLD carbon films containing nitrogen.[21] The peak line shape shows asymmetry and high intensity out to 1400 cm^{-1}, which is distinctly different than the line shape of pure carbon films deposited using PLD of graphite at high (~ 40 J/cm^2) laser energy densities, which typically shows a narrower, more symmetrical peak at ~ 1570 cm^{-1}.[21] This enhancement in peak intensity at lower wave numbers is illustrated by fitting the broad peak with multiple components associated with the vibrational modes of a variety of carbon ring structures. Using the vibrational frequencies computed theoretically for isolated 5, 6, and 7-member carbon rings by Doyle and Denison[22] and vibrational frequencies of 1360 cm^{-1} and 1600 cm^{-1} for the A_1 and E_2 modes of 6-member rings in nanocrystalline graphite, the relative intensities of contributions from pure graphite-like bands and other carbon ring structures (5- and 7-member ring structures in the present case) are obtained, see main panel of Fig. 3.4. The broad peak is dominated by the lower frequency contributions. For these BCN films, a likely explanation for the lower frequency non-graphite vibrational bands are B and/or N-substitution in carbon structures. The hypothetical stable structure for h-BC_2N,[4] which consists of alternating C_2 and BN chains in a graphite-like structure, is one example of such a B, N-substituted carbon structures (to our knowledge, the expected vibrational frequencies for the hypothetical BC_2N structure have not been calculated).

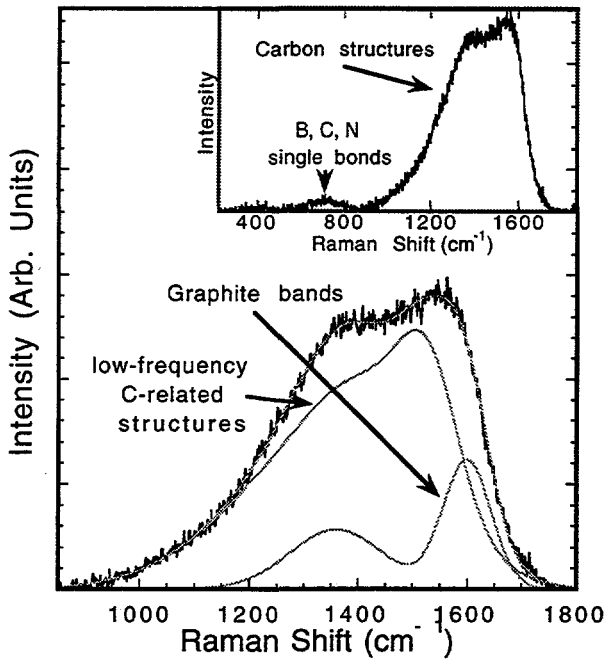

Fig. 3.4. Raman spectrum of a BCN film prepared by PLD from a composite graphite/h-BN target with no N ion irradiation and a substrate temperature of 300°C. The inset shows the complete spectrum, while the main panel shows detail of the carbon-related peak near 1200 - 1700 cm^{-1}. The lightly shaded lines represent numerical fits to this peak assuming vibrational frequencies for graphite and lower vibrational frequency carbon-related structures (e.g. 5- and 7-membered carbon rings). The small peak near 500 - 800 cm^{-1} in the inset is likely related to B-C, B-N, C-N, etc. bonds.

BCN samples containing higher percentages of B and N show greater intensity at lower frequencies for the dominant Raman peak (the dominant peak position shifts from ~ 1560 cm^{-1} to ~ 1430 cm^{-1}). This is suggestive of an even greater degree of B or N substitution into carbon-related structures. B-substitution into carbon structures may be expected to lower vibrational frequencies by lowering the average bond order in p-bonded carbon structures due to a reduction in the total number of valence electrons available for bond formation. Alternatively, lower vibrational frequencies are expected for any B or N substitution which leads to lower strain energy in the bonds.

The broad peak near 500 - 800 cm^{-1} in the Raman spectrum occurs at a position for a number of possible vibrational bands for compounds containing single B-C, B-N, C-N bonds. This peak was enhanced for samples containing a higher percentage of B and N, which suggests that bonding between these elements and carbon constitutes a significant fraction of the peak intensity in this region. Some slight intensity was also observed at ~ 2220 cm^{-1} in BCN films deposited under N ion irradiation, particularly at low substrate deposition temperatures. These high frequency vibrational modes are likely associated with triply-bonded structures, e.g. C≡C or C≡N.

Raman spectroscopy of BCN samples has only occasionally been employed. Andreev et al. have observed Raman bands for nitrided B_4C at 1332 - 1336 cm^{-1} and other bands near 1553 cm^{-1} which were attributed to h-BN derived and graphite derived features, respectively.[19] As also found here, however, the peak positions were shifted from their bulk analogs, suggesting some compositional intermixing.

The electrical properties of the BCN films were investigated by resistivity measurements normal to the film plane and field emission measurements from the surface of the films. Resistivities were measured at room temperature from the current-voltage (I-V) characteristics across the thickness of the film. All samples were found to be conductive, exhibiting ohmic behavior and typical resistivities ranging from ~ 1 x 10^2 Ωcm to 1 x 10^3 Ωcm. In general, the most resistive samples were found for samples deposited at ~ 25°C from the composite graphite/h-BN target, and the most conductive samples were those BCN films deposited at high temperature, ~ 300°C, using either the B_4C or composite targets. In this measurement geometry, the resistivities are particularly sensitive to the presence of any conductive phases in the film which can short the bottom and top contacts. Two-point resistivity measurements made on one sample deposited on to an insulating substrate (sapphire) indicated a resistivity in the plane of the film of ~ 2.5 x 10^3 Ωcm (assuming negligible contact resistance for the Au wire probes). This is close to the resistivity normal to the film, which, at a minimum, suggests that the conductive component to the films are well-connected and well-distributed throughout the film (e.g. above the percolation threshold). Most samples showed spalling on the sapphire substrates, so few in-plane resistivity measurements were performed. It is interesting to note that the deposition of films using PLD from graphite targets or h-BN targets separately leads to amorphous tetrahedrally coordinated films (a-tC) or c-/h-BN films with resistivities > 10^7 Ωcm and > ~ 10^{13} Ωcm, respectively.[23] Clearly, the conductive BCN films fabricated by deposition from the mixed graphite/h-BN target are not simple mixtures of a-tC and c-/h-BN, rather there must be atomic-level mixing of the constituents leading to the higher conductivities (classical doping effects are unlikely given the always high atomic concentration of the minor component).

The similarity in measured resistivities amongst the various BCN samples suggests the conductive phase in each of the films may be similar. One potential source for the conductive component to the films is carbon alloys with boron or nitrogen. Electrical measurements of "nitrogen-doped" carbon films deposited by PLD of graphite at room temperature in an ambient of 10 mTorr N_2 (N content in the films up to ~ 30%) show a marked drop in resistivity with respect to the "undoped films", from > 10^7 Ωcm down to 10 to 10^2 Ωcm.[23] This is a similar resistivity range as observed for the BCN films. The resistivities for the BCN films in this work tend to be higher than those reported for other BCN films. Reported resistivities for CVD BCN thin films range from < 10^{-1} Ωcm[24][25] to ~ 2 Ωcm[26] up to 2 x 10^3 Ωcm.[11] For BCN films deposited using PLD with deposition conditions similar to those reported here, Pryor has reported film resistances for 150 nm thick films of 6 - 80 x 10^3 Ω, which roughly correspond to film resistivities of ~ 0.2 to 2 Ωcm.[3] In general, the lower film resistivities are observed for BCN films deposited or processed at higher temperatures, and this is probably related to increased crystallization of the

conductive graphite-like components and/or a reduction of the amount of tetrahedrally coordinated (diamond-like) carbon within the films.

Additional insight into the electrical properties of the BCN films was obtained by field emission measurements. In brief summary, representative samples from both the carbon-rich end of the BN-C tie line (e.g. a sample deposited using the composite graphite/h-BN target without N ion irradiation) and samples near the carbon-deficient end of the BN-C tie line (e.g. a sample deposited using the B_4C target and N ion irradiation) were examined. Electrical contact to the film was made via the W metal layer beneath the film and a stainless steel ball, 2 mm in diameter suspended 20 - 50 μm above the BCN surface was used as the anode. Details of the measurements are described elsewhere.[27] Fig. 3.5 shows typical I-V emission spectra for the C-rich and C-deficient BCN films, along with a typical emission spectrum for a pure carbon film deposited by PLD from a graphite target (the current at high field is limited by a 2 MΩ ballast resistor in series with the cathode). Pryor has measured the initiation of electron emission for BCN films apparently within the composition range of the BCN films measured here and found extremely low turn-on voltages (< 1 V/μm).[3] These emission characteristics would be much better than those of any other non-surface treated (e.g. non-cesiated) cold cathode emitting material that we are aware of. In contrast to Pryor's results, we find that the turn-on voltages for both compositions of BCN films measured here are not extremely low and are, in fact, higher than those of comparable cold cathode emitters, e.g. carbon films deposited by PLD. The turn-on voltage for the carbon-rich BCN film is high, > 120 V/μm, while the turn-on voltage for the carbon-deficient film BCN film is much lower, ~ 50 V/μm. A typical PLD carbon film deposited by ablation from a graphite target at 5 J/cm^2 in vacuum has a turn-on voltage lower still of ~ 20 V/μm.[27] Recently, even lower turn-on voltages have been reported for nitrogen containing hydrogenated amorphous carbon films, down to as low as 4 V/μm.[28]

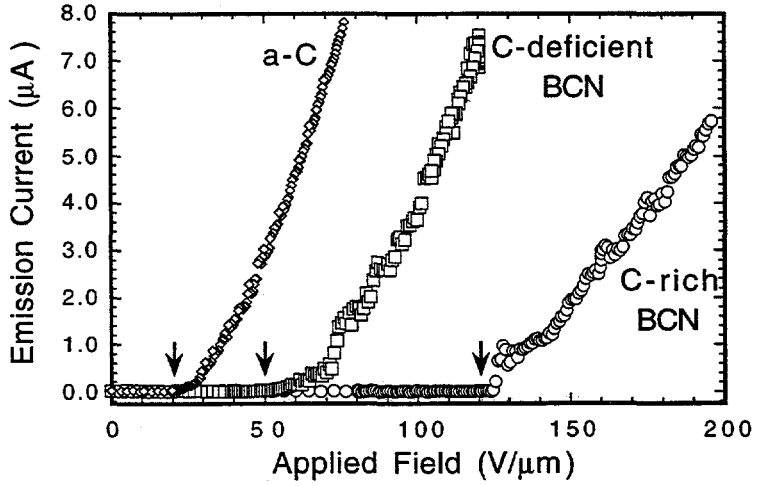

Fig. 3.5. Field emission current as a function of applied field for a carbon-rich BCN film (deposited by PLD using a composite graphite/h-BN target), a carbon-deficient BCN film

(deposited by PLD using a B_4C target with N ion irradiation), and an amorphous carbon film (deposited using PLD from graphite at a laser fluence of ~ 5 J/cm^2). A ballast resistor in series with the samples limits the current at high fields. The arrows represent the "turn-on" threshold of electron emission.

The mechanism for field emission in carbon-related materials is still unresolved. While the work function at the surface may be important, equally important are the geometry, morphology (including sample heterogeneity), and conductivity of the emitting material. While field emission from BCN films may be readily obtained, we have not found the films to be substantially better emitters than pure carbon films. Since the electrical measurements are suggestive of the presence of a B- or N-"doped" conductive carbon component to the film, some of the field emission characteristics may be related to this component of the film. It is interesting to note, however, that the C-deficient films are apparently better emitters, which is contrary to expectation. The C-deficient films, which were deposited from the B_4C target with N ion irradiation, contain higher particle densities on the surfaces (related to higher particle generation from the B_4C target). Whether this has an effect on the field emission properties is under investigation (it should be noted, however, that geometrical field enhancement of emission is unlikely due to the small particle size and large film to anode separation).

In summary, the local atomic bonding in BCN films is difficult to assess. BCN films deposited using PLD with B_4C targets and N ion irradiation or composite graphite/h-BN targets with and without N ion irradiation show similar bonding properties despite their dissimilar compositions. Our measurements indicate that the bonding is likely heterogeneous, but on an extremely fine length scale (a few nm). The evidence for the various bonding structures is outlined below:

(1) Transmission electron diffraction indicates the samples have a layered structure, with similar electron diffraction to turbostratic graphite, turbostratic BN, or h-BCN. Some c-BN bonding may also be present, however.

(2) FTIR indicates vibrational modes which are similar to those of h-BN. Vibrational modes characteristic of c-BN are present in some films, but B-C vibrational modes, which occur at the same frequency range, are also possible. The BN-like modes appear stronger in BN-rich BCN films.

(3) Raman spectroscopy shows fluorescence characteristic of BN films for the BN-rich BCN films. All samples show strong peaks characteristic of carbon structures, particularly carbon π-bonded or 3-fold coordinated structures with B and/or N substitution. B, C, and/or N singly-bonded structures also seem to be present, as well as triply bonded C≡C or C≡N.

(4) Electrical characterization indicates the presence of a pervasive conductive component to the films. Measured resistivities are similar to those of N-containing carbon films deposited by PLD.

(5) Field emission properties are similar to those of other carbon-related films, and do not appear to be a dramatic improvement over other materials.

Because these BCN films are deposited far from equilibrium, there is probably no single local bonding structure which adequately depicts the true bonding and properties. Instead, it is likely, that the films possess a few bonding structures, with h-BN and conductive, B- or N-

"doped" carbon being the dominant bonding manifestations. The high conductivities observed for all BCN compositions indicates that it is unlikely that any suitable low k dielectric can be synthesized from ternaries of B, C, and N.

†In collaboration with T. A. Friedmann, N. Missert, D. R. Tallant, P. P. Provencio, J. C. Barbour, S. C. Fleming, M. L. Lovejoy, and S. R. Kurtz.

References

1. R. Riedel, Adv. Mater. **6**, 549 (1994).
2. M. Morita, T. Hanada, H. Tsutsumi, Y. Matsuda, and M. Kawaguchi, J. Electrochem. Soc. **139**, 1227 (1992).
3. R. W. Pryor, Appl. Phys. Lett. **68**, 1802 (1996).
4. A. Y. Liu, R. M. Wentzcovitch, and M. L. Cohen, Phys. Rev. B **39**, 1760 (1989).
5. W. R. Lambrecht and B. Segall, Phys. Rev. B **47**, 9289 (1993).
6. M. O. Watanabe, S. Itoh, K. Mizushima, and T. Sasaki, Appl. Phys. Lett. **68**, 2962 (1996).
7. Y. G. Andreev, T. Lundström, R. K. Harris, S.-W. Oh, D. C. Apperley, and D. P. Thompson, J. of Alloys Comp. **227**, 102 (1995).
8. M. Hubácek and T. Sato, J. Sol. State Chem. **114**, 258 (1995).
9. S. Nakano, M. Akaishi, T. Sasaki, and S. Yamaoka, Chem. Mater. **6**, 2246 (1994).
10. J. Kouvetakis, T. Sasaki, C. Shen, R. Hagiwara, M. Lerner, K. M. Krishnan, and N. Bartlett, Synth. Met. **34**, 1 (1989).
11. R. B. Kaner, J. Kouvetakis, C. E. Warble, M. L. Sattler, and N. Bartlett, Mat. Res. Bull. **22**, 399 (1987).
12. T. A. Friedmann, P. B. Mirkarimi, D. L. Medlin, K. F. McCarty, E. J. Klaus, D. R. Boehme, H. A. Johnsen, M. J. Mills, D. K. Ottesen, and J. C. Barbour, J. Appl. Phys. **76**, 3088 (1994).
13. J. P. Sullivan, J. C. Barbour, T. A. Friedmann, and S. C. Fleming, unpublished.
14. T. Sasaki, M. Akaishi, S. Yamaoka, Y. Fujiki, and T. Oikawa, Chem. Mater. **5**, 695 (1993).
15. F. Saugnac, F. Teyssandies, and A. Marchans, J. Phys. IV, Suppl. C2 **1**, C2-673 (1991).
16. A. Weber, U. Bringmann, R. Nikalski, and C.-P. Klages, Diamond and Relat. Mater. **2**, 201 (1993).
17. L. Maya and L. A. Harris, J. Am. Ceram. Soc. **73**, 1912 (1990).
18. JCPDS-ICDD Powder Diffraction Files nos. 25-284, 34-421, 25-1033, and 35-1292.
19. Y. G. Andreev and T. Lundström, J. Alloys Comp. **210**, 311 (1994).
20. D. R. Tallant, private communication.
21. T. A. Friedmann, D. R. Tallant, J. C. Barbour, J. P. Sullivan, M. P. Siegal, R. L. Simpson, and J. Mikkalson, Mat. Res. Soc. Proc. **388**, 393 (1995).
22. T. E. Doyle and J. R. Dennison, Phys. Rev. B **51**, 196 (1995).
23. J. P. Sullivan, P. B. Mirkarimi, K. F. McCarty, T. A. Friedmann, L. J. Martinez-Miranda, N. Missert, M. P. Siegal, and M. L. Lovejoy, to be published.
24. M. O. Watanabe, S. Itoh, K. Mizushima, and T. Sasaki, J. Appl. Phys. **78**, 2880 (1995).
25. A. W. Moore, S. L. Strong, G. L. Doll, M. S. Dresselhaus, I. L. Spain, C. W. Bowers, J. P. Issi, and L. Piraux, J. Appl. Phys. **65**, 5109 (1989).
26. L. Maya, J. Electrochem. Soc. **135**, 1278 (1988).
27. N. Missert, T. A. Friedmann, J. P. Sullivan, and R. G. Copeland, Appl. Phys. Lett., 1997.
28. G. A. J. Amaratunga and S. R. P. Silva, Appl. Phys. Lett. **68**, 2529 (1996).

IV. Thermal Stability of Fluorinated SiO_2 Films: Effects of Hydration and Film-Substrate Interaction†

Fluorinated SiO_2 (SiOF) films have emerged as a leading candidate to replace SiO_2 as an interlevel dielectric (ILD) for future ultra-large scale integrated microelectronics.[1] It is acknowledged, however, that SiOF films can exhibit instability problems, particularly in their tendency for moisture absorption.[2] The tendency for moisture absorption is very sensitive to the deposition process and deposition conditions. It is generally observed that SiOF films that are deposited using a high density plasma process [e.g. electron cyclotron resonance (ECR) or helicon plasma chemical vapor deposition (CVD)] produce SiOF films with improved degradation resistance, possibly due to preferential elimination of weakly-bonded F.[3] Further improvement is obtained by using an electrical bias between the substrate and plasma[4] and depositing the SiOF films at elevated temperature.[5] Even though these processes lead to significant improvements in degradation resistance, the ultimate stability of these films when integrated with Al interconnects and other microelectronic materials is not fully known. In this study, the thermal stability of SiOF films deposited using ECR CVD with a biased substrate at elevated temperature was examined as a function of both F content and substrate type.

The SiOF films were deposited in an ECR plasma reactor using a gas mixture of SiH_4, SiF_4, O_2, and Ar. The F content of the films was controlled by adjusting the ratio of flow rates, SiH_4:SiF_4, from 0:1 to 4.7:1, yielding films with F contents ranging from 11% to approx. 2.5%, respectively (as measured by Rutherford Backscattering Spectroscopy, RBS). The microwave power used to excite the plasma was 1500 W and the RF bias power from substrate to plasma was 2300 W. The substrate temperature was 330°C. These conditions have previously been found to lead to SiOF films with excellent thermal stability on Si.

Four types of substrates were used in this study: high resistivity Si, Al(0.29 to 0.7 μm)/Si, TiN(0.05 μm)/Al(0.7 μm)/Si, and Al(1.0 μm)/SiO_2(1.0 μm)/Si. The thick Al layers were sputter deposited at 100°C with an intentional Si-doping of 0.75%. For most of the samples, the SiOF deposited layer was 0.15 to 0.19 μm thick, and all measurements were taken approx. 2 to 14 days after film deposition and unloading (outside the deposition system, the samples were exposed to normal room ambient conditions). For a few samples, identified as "thick SiOF", the SiOF layer was much thicker, 0.8 to 0.9 μm, and the measurements were taken more than 6 mos. after film deposition and unloading.

"Hydration" treatments were performed by boiling the samples in distilled H_2O for one hour (95°C and 690 Torr). All annealing treatments were performed at 400°C, in vacuum (2×10^{-6} Torr), for 30 min., unless otherwise noted. Other annealing ambients (forming gas or Ar) gave similar results to those found for the vacuum anneals. The annealing temperature was chosen to approximate the thermal budget the SiOF films would need to withstand during processing as an IMD.

Electrical characterization was performed on the SiOF layers on the metallized substrates.

(High interface state densities and high substrate resistivities prevented accurate determination of the SiOF film capacitance for layers deposited on Si substrates.) Contact was made to the metal layer beneath the SiOF by photoresist masking and reactive ion etching through the SiOF. Shadow mask deposition of circular Ti/Au contacts were made to the top surface of the films with diameters ranging from approx. 200 μm to 1000 μm. Uncertainties in the measurement of film capacitance changes following annealing were greatly reduced by measuring the exact same contacts immediately prior and following the anneal step.

Ellipsometry and Fourier Transform Infrared (FTIR) spectroscopy were performed on SiOF layers on Si substrates. RBS and elastic recoil detection (ERD) of hydrogen were performed on samples on all types of substrates. High resolution transmission electron microscopy (HRTEM) and nanoprobe energy dispersive analysis by X-rays (EDAX) were performed on SiOF layers on Al- and TiN-coated substrates. These latter samples were prepared by mounting the samples film surface to film surface, mechanical thinning, and ion milling to electron transparency (< 50 nm thick).

Moisture absorption is known to be a concern in SiOF films.[1-10] In order to quantify this effect in these films, hydration was performed on all films. Fig. 4.1 shows the effect of hydration on the SiO-H absorbance in low and high F content SiOF layers on Si as measured by FTIR. Hydration was found to increase the absorbance in high F (11% F) content layers while only negligible changes were observed in the middle (6%) to low (2.5%) F content films. Despite the increase in SiO-H absorbance, the total absorbance signal was still very small compared to the dominant vibrational modes (< 0.5% of the Si-O peak). A slight drop in the Si-F/Si-O ratio of about 3.3% was also observed in the high F content films following hydration, while negligible changes occurred in the low F content films. There was no noticeable increase in absorbance at frequencies associated with the H-OH stretch of water in all films following hydration.

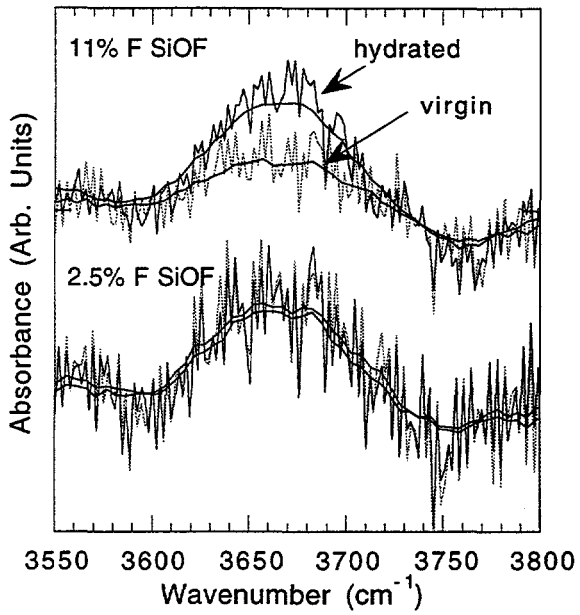

Fig. 4.1. SiO-H absorbance as measured by FTIR before and after hydration for 2.5% and 11% F SiOF films.

The changes which occurred in the film as a result of hydration were not limited to SiOF films on Si. Fig. 4.2 shows the hydrogen increase in an 11% F content SiOF layer on Al/Si as detected by ERD. ERD measures H from all sources, including Si-OH bonds, Si-H, and trapped H_2O. While the H concentration of the virgin (un-hydrated) samples which were analyzed 2 to 14 days after film deposition were all similar, the H content of thick SiOF films deposited > 6 mos. before analysis were higher, being approximately 2% for the low F (2.3% F) films and 3% for high F (11% F) films. This suggests that exposure to room ambient conditions is sufficient to lead to hydration over time. After annealing the hydrated films, no noticeable change in absorption at 3660 cm^{-1} was found, as shown in Fig. 4.3. This is consistent with thermal desorption spectra (TDS) for plasma-enhanced CVD SiO_2 films in which no significant changes were observed in the SiO-H absorbance until the anneal temperature exceeded 400°C.[11]

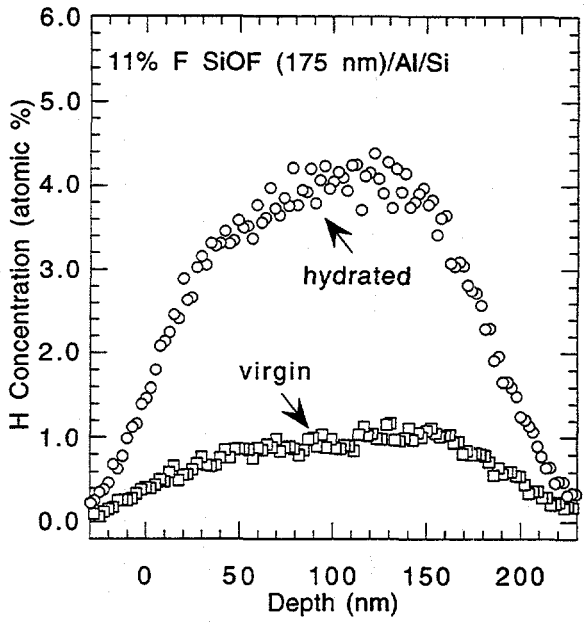

Fig. 4.2. Atomic H concentration in an 11% F SiOF film on Al/Si before and after hydration.

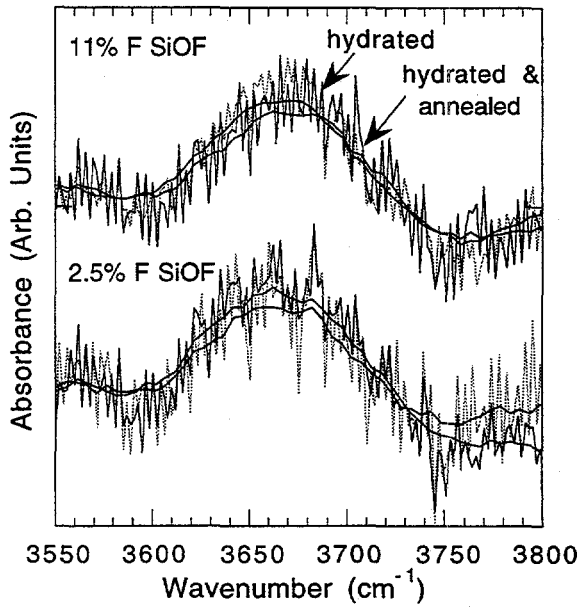

Fig. 4.3. SiO-H absorbance for hydrated SiOF films before and after annealing.

The effect of the moisture-induced instability was determined by measuring capacitance changes in the SiOF layers following annealing. Table 4.1 summarizes the capacitance changes for high F content films as a function of substrate type, F content of the film, and anneal temperature. It was found that all high F content films exhibited a decrease in capacitance following annealing independent of substrate type. The capacitance drop was dependent on the F content of the film,

however, as shown in the middle section of the table. For low F content films, a slight capacitance increase was observed. Finally, it was observed that the capacitance change following annealing began to show noticeable changes following the 200°C anneal. Since slight thickness changes in the SiOF film could be responsible for the observed capacitance changes, ellipsometry was performed on SiOF layers deposited under identical conditions to those above except on Si substrates. Changes in film thickness following annealing or hydration and annealing were found to be less than 1% (typically a slight decrease was observed, but the changes were close to the estimated uncertainty of the measurement, ~ 0.4%). This is not sufficient to explain the observed capacitance changes, although it might explain part of the capacitance increase for the low F content films. Given that the observed onset for capacitance changes was 200°C, a likely explanation for the capacitance drop is desorption of H_2O in the films. TDS indicates that the only significant desorption species near 200°C for SiOF films is weakly-bound H_2O.[4] Blistering of the metal contacts to the thick 11% F SiOF layer on Al/Si was also found to occur starting after the 200°C anneal. This would also support the desorption of H_2O as the likely mechanism. Due to the blister formation, no accurate measurement of the capacitance reduction of the thick SiOF layers on Al/Si could be obtained. The small capacitance drop observed in the thinner SiOF films may be a result of either the formation of a void beneath the metal contact of a size too small to be observed as a blister or merely the loss of the highly polarizable, weakly-bound H_2O species from the film. In either case, the electrical measurements support the FTIR and ERD measurements that moisture absorption in the SiOF films increases with increasing F content and that the degree of moisture absorption appears to be independent of substrate type.

Table 4.1. Capacitance change following annealing, referenced to unannealed samples, as a function of substrate type, F content, and anneal temperature.

A. Dependence on Substrate		B. Dependence on F Content		C. Dependence on Anneal Temp.	
Sample	Cap. Change	Sample	Cap. Change	Sample	Cap. Change
11% F SiOF/Al/Si	-2.4%	11% F SiOF/Al/SiO_2/Si	-3.3%	11% F SiOF/Al/Si annealed 100°C	-0.2%
11% F SiOF/TiN/Al/Si	-2.3%	6% F SiOF/Al/SiO_2/Si	-0.3%	11% F SiOF/Al/Si annealed 200°C	-1.1%
11%F SiOF/Al/SiO_2/Si	-3.3%	2.5% F SiOF/Al/SiO_2/Si	+1.8%	11% F SiOF/Al/Si annealed 300°C	-2.1%
				11% F SiOF/Al/Si annealed 350°C	-2.7%
				11% F SiOF/Al/Si annealed 400°C	-2.7%

Although the moisture absorption instability of SiOF films seemed only to depend on the F content of the layer and not on the type of substrate, it was found that there is an instability associated with F loss from the film which does appear to depend on the type of substrate. The F/O ratio in SiOF films was measured by nanoprobe EDAX with a 10 nm spot size. Point composition measurements were taken from the middle of the SiOF layer working towards the SiOF/substrate interface. These composition profiles are shown in Fig. 4.4. It was observed that

there is noticeable loss of F with respect to the oxygen signal for annealed thick SiOF films on Al/Si substrates when compared to the unannealed films [Fig. 4.4(a)]. This F loss was also found for the thinner SiOF films on the Al/Si substrate [Fig. 4.4(b)], but no detectable loss was found for the SiOF films on the TiN/Al/Si substrates.

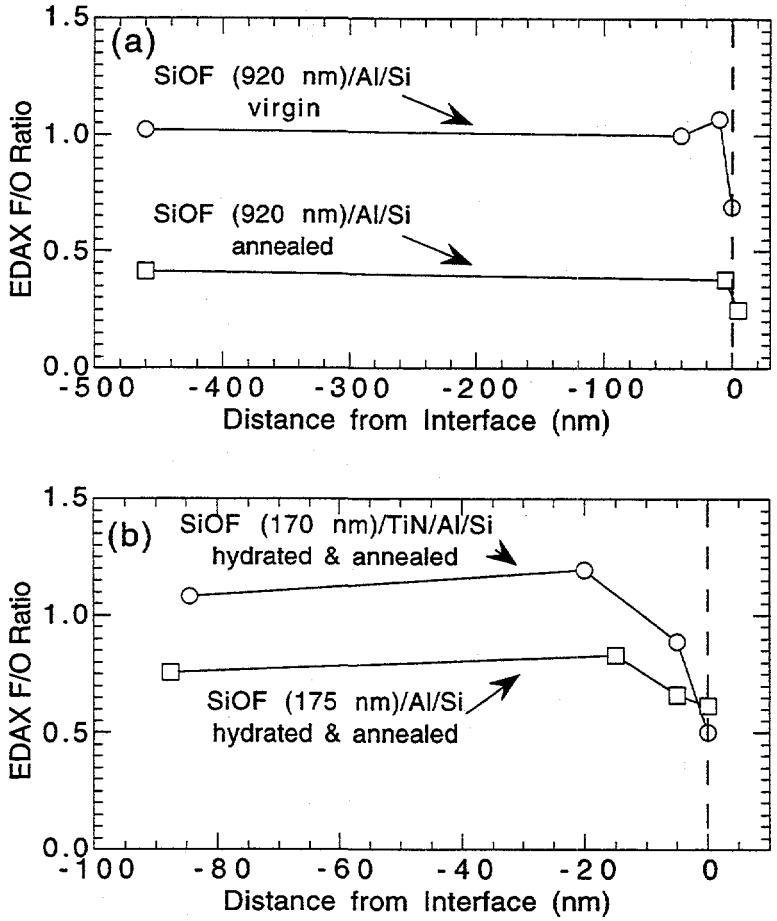

Fig. 4.4. Measured F/O ratios within SiOF films as determined by EDAX (uncorrected for cross-section differences between F and O) as a function of distance from the metal interface for (a) thick SiOF films on Al/Si and (b) SiOF films on TiN/Al/Si and Al/Si. A reduction in F content is observed for annealed films on Al/Si substrates.

RBS confirms the EDAX observations, as indicated in Table 4.2. It does appear that moisture absorption is also important for this reaction to proceed because less F is lost for the 11% F SiOF layer on Al/Si after receiving only an annealing treatment compared to the same film after both a hydration and annealing treatment, see Table 4.2 (the thick SiOF films behave as hydrated films following 6 mos. exposure to room ambient conditions). Little or no change in F content was also found for 11% F SiOF layers on Si following hydration and annealing as indicated by measurement of the change in Si-F/Si-O ratio (a decrease of about 5% was found). In summary, the only systems which showed noticeable F reduction were the systems in which there was a high F content SiOF layer on Al/Si. This highlights a potential difficulty when assessing the thermal

stability of SiOF layers in contact with Al by only monitoring changes in SiOF layers on Si substrates.

Table 4.2. Percent F reduction in SiOF films as measured by RBS following the specified treatment and referenced to the untreated sample. Reductions of less than approx. 5% are labeled as "small" or "none".

Sample	Treatment	% F Reduction
thick SiOF/Al/Si, 11% F	annealed	25%
thick SiOF/Al/Si, 2.3% F	annealed	none
SiOF/Al/Si, 11% F	hydrated and annealed	18%
SiOF/Al/Si, 11% F	annealed	small to none
SiOF/TiN/Al/Si, 11% F	hydrated and annealed	none
SiOF/Al/SiO_2/Si, 11% F	hydrated and annealed	small to none

The mechanism for the loss of F from annealed SiOF layers in contact with Al/Si substrates is unclear. It is generally accepted that the F in the SiOF films is directly bonded to the Si, as is supported by theoretical calculations involving small $Si_wO_xF_yH_z$ clusters.[12] Assuming the free energy for bond breakage of the F-Si≡ bond in the SiOF solid is similar to that of bond breakage in the F-SiF_3 molecule, then simple thermodynamic arguments rule out direct reactions between H_2O and SiF_4 to yield SiO_2 [or $Si(OH)_4$] and HF:[13]

(1) $SiF_4 + 2H_2O \rightarrow SiO_2 + 4HF$ $\Delta G°$ (298 K) = +23.3 kcal/mol

(2) $SiF_4 + 4H_2O \rightarrow Si(OH)_4 + 4HF$ $\Delta G°$ (298 K) = +22.8 kcal/mol

Because Al is more electropositive than Si, stripping of F from Si by Al is possible:

(3) $3SiF_4 + 4Al \rightarrow 3Si + 4AlF_3$ $\Delta G°$ (298 K) = -8.36 kcal/mol

This reaction does not appear operative, however, because the F profile as measured by EDAX showed no significant increase near the SiOF/Al interface. Other possibilities include $Al(OH)_3$ formation at the SiOF/Al interface due to reaction between Al and H_2O with subsequent release of H_2. H release from the Al layer or catalytic reactions at the Al interface are also possible. Finally, it is not understood why the F loss from the SiOF layer is different for the Al/Si substrates compared to the Al/SiO_2/Si substrates, as indicated in Table 4.2. This difference could be related to differences in H content between the Al layers in these films, but that difference has not been measured.

In order to reduce the two types of instability problems associated with SiOF films in contact with Al, it is advisable to employ moisture barrier layers, such as F-free SiO_2 layers or Si_xN_y layers on the top surface of the film and use a diffusion barrier, such as TiN, between the SiOF film and the Al interconnect. It is interesting to note that these two approaches, the use of a moisture barrier layer, Si_xN_y, and a Ti barrier layer between the Al and the SiOF, have already been tested experimentally and were found to reduce the degradation observed in Al lines when integrated with SiOF.[8]

In summary, two types of thermal instability problems were observed for SiOF films. One instability problem is related to moisture absorption which increased with increasing F content and was independent of the type of substrate upon which the SiOF was deposited. The other instability

problem was due to the loss of F from the SiOF film for films that were deposited on Al/Si substrates and annealed. It is suggested that the use of a moisture barrier layer and diffusion barrier, such as TiN, should eliminate these instability problems. Provided adequate controls are used to prevent these instability problems, SiOF films should be suitable as an intermediate low k dielectric – a bridge between current technology and future dielectrics with substantially lower dielectric constant.

†In collaboration with J. C. Barbour, D. R. Denison, P. P. Provencio, C. A. Apblett, C. H. Seager, and A. G. Baca.

References

1. T. Homma, J. Non-Cryst. Solids **187**, 49 (1995).
2. T. Homma, Thin Solid Films **278**, 28 (1996).
3. M. J. Shapiro, S. V. Nguyen, T. Matsuda, and D. Dobuzinsky, Thin Solid Films **270**, 503 (1995).
4. T. Tamura, Y. Inoue, M. Satoh, H. Yoshitaka, and J. Sakai, Jpn. J. Appl. Phys. **35**, 2526 (1996).
5. K. M. Chang, S. W. Wang, C. J. Wu, T. H. Yeh, C. H. Li, and J. Y. Yang, Appl. Phys. Lett. **69**, 1238 (1996).
6. H. Kitoh, M. Muroyama, M. Sasaki, M. Iwasawa, and H. Kimura, Jpn. J. Appl. Phys. **35**, 1464 (1996).
7. H. Kudo, R. Shinohara, S. Takeishi, N. Awaji, and M. Yamada, Jpn. J. Appl. Phys. **35**, 1583 (1996).
8. B. K. Hwang, J. H. Choi, S. Lee, K. Fujihara, U.-I. Chung, S.-I. Lee, and M.-Y. Lee, Jpn. J. Appl. Phys. **35**, 1588 (1996).
9. P. W. Lee, S. Mizuno, A. Verma, H. Tran, and B. Nguyen, J. Electrochem. Soc. **143**, 2015 (1996).
10. V. L. Shannon and M. Z. Karim, Thin Solid Films **270**, 498 (1995).
11. N. Hirashita, S. Tokitoh, and H. Uchida, Jpn. J. Appl. Phys. **32**, 1787 (1993).
12. A. Yokozawa, K. Hirose, A. Ishitani, M. Kamoshida, S. Hillenius, G. Gilmer, and K. Raghavachari, J. Appl. Phys. **77**, 6345 (1995).
13. data from CRC Handbook of Chemistry and Physics (CRC Press, Boca Raton, FL, 1988).

V. Plasma-Polymerized Fluorocarbon†

Polymeric dielectrics offer some of the greatest promise for achieving ultra-low dielectric constants (2.0 - 3.0).[1] They owe their low permittivity to their low densities, with typical densities substantially lower than most inorganic solid-state materials, e.g. < 2 g/cm^3. While low dielectric constant polymeric materials may be synthesized quite readily, it is significantly more difficult to meet the other requirements for ILDs, high thermal stability (up to 400°C) and high dimensional stability, in particular. A common approach to improving the thermal stability of polymers is to replace the hydrogen groups with fluorine. This is not always sufficient, however. For example, poly(tetrafluoroethylene) possesses both low dielectric constant and reasonable thermal stability, but is considered too mechanically soft and poorly adhering to be considered a suitable ILD.

There are many potential low k polymeric dielectrics under evaluation, including polyimides, fluorinated polyimides, fluorinated poly(arylethers), Si-based polymers (fluorinated silsesquioxanes), etc. As is the case for deposited inorganic films, the deposition and synthesis process for organic films can greatly influence the dielectric constant due to changes in film density.[2] In this study, we have focused on films deposited by a plasma deposition process, plasma polymerized fluorocarbons (PPFC). These are organic, polymer-like materials which are chemically compatible with Si processing. They also have the advantage that they contain negligible H_2O or chemical solvents because of the dry deposition process, and this makes the films less susceptible to shrinkage or outgassing (a common problem for "wet" prepared organic films). The film synthesis is achieved by creating a plasma within a fluorocarbon/inert gas mixture with excitation either by RF, electron cyclotron resonance (ECR), helicon wave, etc. The plasma induces dissociation of the fluorocarbon molecule into active radicals which migrate to the substrate and incorporate into the growing film either by attachment onto a chain end or insertion into an existing chain. Because there may be many reactive end groups for polymerization, the resulting organic film tends to be heavily cross-linked with few long unbranched chain units. Cross-linking is a desirable feature for a low k polymeric dielectric. Cross-linking increases the glass transition temperature which improves thermal stability and increases the stiffness of the material which improves dimensional stability.

In this work we have created plasma polymerized fluorocarbon (PPFC) films in a parallel plate CVD reactor using C_3F_6 as the reagent gas in a background of Ar. C_3F_6 is not the only fluorinated molecule which may be used; CF_4 and mixtures of CF_4 and CH_4 also work.[3,4] In our case, deposition was performed at room temperature on Si substrates or metallized (250 nm W on 1 μm SiO_2) Si substrates. Typical film thicknesses ranged from 1000 to 2000 Å. Dielectric characterization was performed by measuring DC conductivities and AC admittances using metal-insulator-metal structures created by shadow mask deposition of Ti-Au contacts on to the PPFC films deposited on metallized substrates.

Fig. 5.1. shows measured dielectric constants for PPFC films using C_3F_6 compared to PPFC films deposited by Endo and Tatsumi using CH_4 and CF_4 mixtures.[3] For PPFC-C_3F_6

films, we observe dielectric constants in the range of 2.5 to 3.0. This is higher than the dielectric constant obseved by Endo and Tatsumi for their ~ 100% CF_4 films. This difference in dielectric constant is likely a result of different film densities.

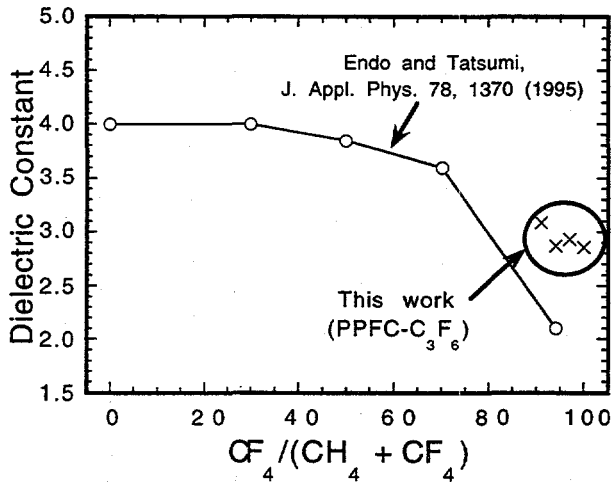

Fig. 5.1. Dielectric constants of PPFC-C_3F_6 films compared to plasma-deposited films created from CH_4/CF_4 mixtures by Endo and Tatsumi, Ref [3].

In addition to having low dielectric constant, PPFC-C_3F_6 films are also highly insulating, as shown in Fig. 5.2. A typical figure of merit is the bias voltage required to create a leakage current of 10^{-9} A/cm^2 through the dielectric. The leakage current should be less than 10^{-9} A/cm^2 over the range of bias voltages applied to the metal interconnects. Scaling by the dielectric thickness, this implies that the current density should remain below 10^{-9} A/cm^2 over the bias range of approximately ± 0.4 V, which is easily satisfied by the PPFC-C_3F_6 films.

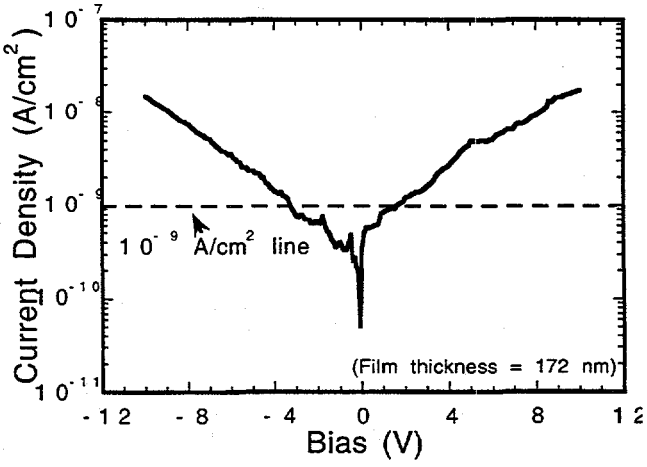

Fig. 5.2. Leakage current as a function of bias voltage for PPFC-C_3F_6 films.

Given the low dielectric constant, high electrical resistance, apparent good thermal and dimensional stability, it would appear that PPFC materials should be good candidates as ILD materials. There is one problem with PPFC materials which is often overlooked, however. Fig. 5.3. shows the dielectric loss (tan δ) in PPFC films as a function of frequency and environmental conditions. Over time and exposure to atmospheric oxygen, PPFC films become increasingly lossy. This degradation is due to the following: (1) an unavoidable consequence of plasma polymerization is that unterminated free radicals are trapped in the film, (2) upon exposure to atmospheric oxygen, oxygen diffuses into the film and reacts with the free radicals to create peroxide radicals, (3) over time the peroxide radicals convert to carbonyl groups, C=O, which are then stable. The reaction sequence is diagramed below.

$$C\bullet + O_2 \rightarrow C-O-O\bullet \rightarrow C=O$$

Carbonyl groups are polar and can contribute to dielectric loss due to increased molecular polarizabilities.

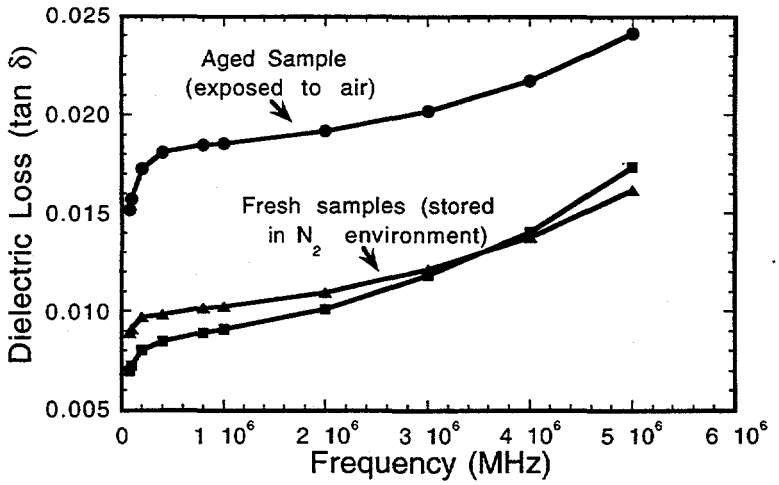

Fig. 5.3. Dielectric loss of PPFC-C_3F_6 films as a function of time and environmental exposure.

PPFC materials could be acceptable ILD materials if the problem with unterminated free radicals during deposition can be resolved. One promising approach involves terminating the free radicals during or immediately subsequent to deposition *prior* to removal of the film from the deposition chamber. Two of the most desirable terminating groups are H and F. The challenge, however, is to develop a passivation procedure in which the active H or F atoms do not themselves contribute to the formation of free radicals by bond scission (e.g. chemical etching or energy transfer from highly energetic H or F atoms). An alternative approach is to deposit the organic film not by a plasma technique, but by thermal dissociation of a fluorinated organic reagent. One example is hot filament deposition of a fluoropolymer using hexafluoropropylene oxide as the monomer.[5]

†In collaboration with R. R. Rye, R. J. Buss, A. G. Baca, and E. L. Venturini.

References

1. N. H. Hendricks, Solid State Technol. **8**, 117 (1995).
2. H. J. Cha, J. Hedrick, R. A. DiPietro, T. Blume, R. Beyers, and D. Y. Yoon, Appl. Phys. Lett. **68**, 1930 (1996).
3. K. Endo and T. Tatsumi, J. Appl. Phys. **78**, 1370 (1995).
4. K. Endo and T. Tatsumi, Appl. Phys. Lett. **68**, 2864 (1996).
5. S. J. Limb, C. B. Labelle, K. K. Gleason, D. J. Edell, and E. F. Gleason, Appl. Phys. Lett. **68**, 2810 (1996).

VI. Summary

In this research program, the feasibility of several candidate low k dielectric materials was examined. Materials were selected which were known to be chemically compatible with Si processing. These included (1) covalently-bonded ceramics comprised of carbon, boron and nitrogen, or a mixture of carbon, boron, and nitrogen; (2) fluorinated SiO_2 films; and (3) plasma polymerized fluorocarbons. The advantages, disadvantages, and critical technical issues facing each of these new material systems are all different, and are discussed below.

Covalently-bonded thin film ceramic materials comprised of carbon, boron and nitrogen, and mixtures of boron, carbon, and nitrogen are an exciting class of new materials. We have examined the structural, physical, and electrical properties of these materials with the aim of assessing their suitability as interlevel dielectrics. It was discovered that it is necessary to use a highly energetic deposition technique, such as pulsed-laser deposition, in order to create films which meet the rigorous demands of thermal and environmental stability. Unfortunately, these energetic deposition techniques also produce films which are denser than those produced by typical plasma deposition techniques. The high densities unavoidably lead to dielectric constants close to the bulk values and too high for optimal use as a low k ILD. This situation can be described as a balance of trade-offs: plasma deposition processes can produce films of low dielectric constant but these films are thermally or environmentally unstable, while highly energetic processes can produce stable films but with dielectric constants which are too high. These latter films, however, show great promise for other applications, such as tribological coatings, micro-sensors, or cold cathode emitters. Stability is not the problem for films containing mixtures of boron, carbon, and nitrogen. These films due not yield acceptable low k ILDs, however, because of the catalytic role that nitrogen plays in stabilizing 3-fold coordinated carbon. 3-fold coordinated carbon is undesirable because it increases the electrical conductivity of the film to levels which are simply too high for a dielectric material.

Fluorinated SiO_2, SiOF, is a very promising ILD material for near-term applications. One reason it is so promising is that the process for deposition of SiOF films is almost completely interchangeable with current processes used to deposit conventional SiO_2 films, thus reducing tooling costs. A disadvantage is that the dielectric constant of SiOF films do not fall below about 3.5, which only represents a 10% improvement over SiO_2. This 10% is significant enough to explore this material for near-term applications until a replacement ILD with even lower dielectric constant can be found. Another disadvantage with SiOF – which may be rectified by proper use of barrier and capping layers – is that the films exhibit instability with regard to moisture absorption and degradation when in contact with Al layers. We have found that the interfacial degradation problem when SiOF films are annealed is unique to Al – no degradation is observed for Si or TiN interfaces. The chemical role played by the Al is not clear, but it apparently enhances F loss from the SiOF films. It is suggested that placing a barrier layer, such as TiN, between the Al and the SiOF should help eliminate this problem.

Plasma polymerized fluorocarbon films, PPFC, can show both low dielectric constant (around 2.5) and good thermal and dimensional stability, at least compared to other polymeric materials. Moreover, the deposition technique is a "dry" process which makes it particularly attractive for ILD deposition. PPFC materials have a unique disadvantage, however. The deposition process leads to the formation of free radicals in the film. These free radicals react with atmospheric oxygen eventually leading to the formation of carbonyl groups which causes the dielectric loss in the film to increase over time. Lossy dielectrics are, of course, undesirable as ILDs because at high frequencies the drive current increases, leading to excessive power consumption, heating, and degradation in reliability. If techniques can be developed to passivate the free radicals in the PPFC films prior to their removal from the deposition chamber, these materials may make effective ILD materials.

The current situation for novel ILD materials is still unclear. Best estimates are that SiOF will be integrated as an interim low k dielectric material to be followed later by some polymeric material (possibly PPFC, fluorinated polyimides, poly(arylethers), fluorinated silsesquioxanes, etc.) with even lower dielectric constant. If the minimum thermal stability temperature for ILDs can be lowered from the 400°C standard, then some existing polymeric dielectrics may already be able to satisfy the requirements for a new low k ILD material.

Distribution:

1	MS-0188	C. E. Myers, 4523
1	MS-1056	J. C. Barbour, 1111
1	MS-1421	E. B. Stechel, 1153
5	MS-1421	J. P. Sullivan, 1153
1	MS-1421	T. A. Friedmann, 1153
1	MS-1421	M. P. Siegal, 1153
1	MS-1421	N. Missert, 1153
2	MS-1427	S. T. Picraux, 1100
1	MS-9018	Central Technical Files, 8940-2
5	MS-0899	Technical Library, 4916
2	MS-0619	Review & Approval Desk, 12690